

# Quaternion Tensor Train Rank Minimization with Sparse Regularization in a Transformed Domain for Quaternion Tensor Completion

Jifei Miao, Kit Ian Kou, Liqiao Yang, Dong Cheng

**Abstract**—The tensor train rank (TT-rank) has achieved promising results in tensor completion due to its ability to capture the global low-rankness of higher-order ( $> 3$ ) tensors. On the other hand, recently, quaternions have proven to be a very suitable framework for encoding color pixels, and have obtained outstanding performance in various color image processing tasks. In this paper, the quaternion tensor train (QTT) decomposition is presented, and based on that the quaternion TT-rank (QTT-rank) is naturally defined, which are the generalizations of their counterparts in the real number field. In addition, to utilize the local sparse prior of the quaternion tensor, a general and flexible transform framework is defined. Combining both the global low-rank and local sparse priors of the quaternion tensor, we propose a novel quaternion tensor completion model, *i.e.*, QTT-rank minimization with sparse regularization in a transformed domain. Specifically, we use the quaternion weighted nuclear norm (QWNN) of mode- $n$  canonical unfolding quaternion matrices to characterize the global low-QTT-rankness, and the  $l_1$ -norm of the quaternion tensor in a transformed domain to characterize the local sparse property. Moreover, to enable the QTT-rank minimization to handle color images and better handle color videos, we generalize KA, a tensor augmentation method, to quaternion tensors and define quaternion KA (QKA), which is a helpful pretreatment step for QTT-rank based optimization problems. The numerical experiments on color images and color videos inpainting tasks indicate the advantages of the proposed method over the state-of-the-art ones.

**Index Terms**—Quaternion tensor train decomposition, quaternion tensor completion, sparse regularization, color image inpainting, color video.

## I. INTRODUCTION

Jifei Miao is with the School of Mathematics and Statistics, Yunnan University, Kunming, Yunnan, 650091, China (e-mail: jifmiao@163.com)

Kit Ian Kou is with the Department of Mathematics, Faculty of Science and Technology, University of Macau, Macau 999078, China (e-mail: kikou@umac.mo)

Liqiao Yang is with the Department of Mathematics, Faculty of Science and Technology, University of Macau, Macau 999078, China (e-mail: liqiaoyoung@163.com)

Dong Cheng is with the Department of Mathematics, Faculty of Arts and Sciences, Beijing Normal University, Zhuhai 519087, China (e-mail: chengdong720@163.com)

**T**ensor provides a natural way to represent multidimensional data. For example, a color image is a third-order tensor, a color video is a fourth-order tensor with an additional index in the time variable. In recent years, low-rank tensor completion (LRTC)-based techniques have made a great success in the application of image and video inpainting [1]–[3]. Generally, the LRTC problem is modeled as

$$\begin{aligned} \min_{\mathcal{X}} \text{rank}(\mathcal{X}) \\ \text{s.t. } P_{\Omega}(\mathcal{X}) = P_{\Omega}(\mathcal{T}), \end{aligned} \quad (1)$$

where  $\mathcal{X} \in \mathbb{R}^{I_1 \times I_2 \times \dots \times I_N}$  is a completed output  $N$ -th order tensor,  $\mathcal{T} \in \mathbb{R}^{I_1 \times I_2 \times \dots \times I_N}$  is the observed  $N$ -th order tensor, and  $P_{\Omega}(\cdot)$  is the projection operator on  $\Omega$  which is the index of observed entries. There are different types of definitions of tensor ranks to characterize the low-rankness of tensors, such as CP rank [4], Tucker rank [5], tubal rank [6], tensor train rank (TT-rank) [7], *etc.* Among these definitions of tensor ranks, the TT-rank recently has shown a powerful capacity for characterizing the correlations between different modes in higher-order tensors, which as a result has achieved great success in LRTC. Given an  $N$ -th order tensor  $\mathcal{X} \in \mathbb{R}^{I_1 \times I_2 \times \dots \times I_N}$ , the TT-rank [8] is defined as

$$\text{rank}_{\text{TT}}(\mathcal{X}) = (\text{rank}(\mathbf{X}_{[1]}), \dots, \text{rank}(\mathbf{X}_{[N-1]})), \quad (2)$$

where  $\mathbf{X}_{[n]} \in \mathbb{R}^{\prod_{j=1}^n I_j \times \prod_{j=n+1}^N I_j}$  denotes the Mode- $n$  canonical unfolding of  $\mathcal{X}$  [7]. Due to the TT decomposition being free from the “curse of dimensionality” [7] and the TT-rank can capture the global correlation of higher-order tensors, researchers have developed a series of methods for TT-rank minimization. For LRTC problem, the authors in [3] proposed two TT-rank minimization models. The first one named SiLRTC-TT minimizes the weighted sum of the convex nuclear norm surrogate of TT-rank, *i.e.*,

$$\begin{aligned} \min_{\mathcal{X}} \sum_{k=1}^{N-1} \alpha_k \|\mathbf{X}_{[k]}\|_* \\ \text{s.t. } P_{\Omega}(\mathcal{X}) = P_{\Omega}(\mathcal{T}), \end{aligned} \quad (3)$$

where  $\alpha_k$  for  $k = 1, 2, \dots, N-1$  are positive parameters. Another one named TMac-TT uses matrix factorization to approximate the TT-rank, *i.e.*,

$$\begin{aligned} \min_{\mathbf{P}_k, \mathbf{Q}_k, \mathcal{X}} \quad & \sum_{k=1}^{N-1} \frac{\alpha_k}{2} \|\mathbf{P}_k \mathbf{Q}_k - \mathbf{X}_{[k]}\|_F^2 \\ \text{s.t. } \quad & P_\Omega(\mathcal{X}) = P_\Omega(\mathcal{T}), \end{aligned} \quad (4)$$

where  $\mathbf{P}_k \in \mathbb{R}^{\Pi_{j=1}^n I_j \times r_k}$  and  $\mathbf{Q}_k \in \mathbb{R}^{r_k \times \Pi_{j=n+1}^N I_j}$  are factor matrices, and  $r_k$  denotes the rank of  $\mathbf{X}_{[k]}$ . For TMac-TT, the estimation of  $r_k$  is a challenging task, which directly affects the algorithm performance [3].

On the other hand, quaternion, as an elegant color image representation tool, has attracted much attention in the field of color image processing [9]–[12]. The quaternion processes a color image holistically as a vector field and handles the coupling between the color channels naturally, which allows the color information of the source image is fully used. Consequently, plenty of low-rank quaternion matrix completion (LRQMC) methods have been proposed in recent years and shown promising results in color image inpainting tasks [11], [13], [14]. Furthermore, as a generalization of LRTC in the quaternion domain, we first proposed low-rank quaternion tensor completion (LRQTC) model in our previous work [15], *i.e.*,

$$\begin{aligned} \min_{\dot{\mathcal{X}}} \quad & \sum_{k=1}^N \alpha_k \|\dot{\mathbf{X}}_{(n)}\|_* \\ \text{s.t. } \quad & P_\Omega(\dot{\mathcal{X}}) = P_\Omega(\dot{\mathcal{T}}), \end{aligned} \quad (5)$$

where  $\dot{\mathcal{X}} \in \mathbb{H}^{I_1 \times I_2 \times \dots \times I_N}$  is a completed output  $N$ -th order quaternion tensor,  $\dot{\mathcal{T}} \in \mathbb{H}^{I_1 \times I_2 \times \dots \times I_N}$  is the observed  $N$ -th order quaternion tensor, and  $\dot{\mathbf{X}}_{(n)} \in \mathbb{H}^{I_n \times \Pi_{j=1, j \neq n}^N I_j}$  denotes the Mode- $n$  unfolding of  $\dot{\mathcal{X}}$  [15]. The model (5) is directly following the definition of Tucker rank, *i.e.*,

$$\text{rank}_{\text{tucker}}(\mathcal{X}) = (\text{rank}(\mathbf{X}_{(1)}), \dots, \text{rank}(\mathbf{X}_{(N)})). \quad (6)$$

However, a conceptual flaw of Tucker rank is that its components are the ranks of matrices constructed based on an unbalanced unfolding scheme (one mode versus the rest). The upper bound for each individual rank is usually small and may not be suitable for describing the global information of a tensor [3]. Based on this consideration, we define the quaternion tensor train (QTT) decomposition of quaternion tensors and the corresponding QTT-rank in this paper. The details can be founded in Section III.

In addition, the low-rank component always indicates that the data in practice also have intrinsically sparse property [16]. One possible approach is to exploit the

sparse information of the complete tensor in some domains, such as the transform domain where many signals have an inherently sparse structure [17], [18]. Motivated by this, in this paper, to utilize the local sparse prior of the quaternion tensor, a general and flexible transform framework is defined. Under the framework, any appropriate quaternion multidimensional discrete transform can be contained. The details can be founded in Section IV-A.

Moreover, to enable the QTT-rank minimization to handle color images and better handle color videos, we generalize KA [3], a tensor augmentation method, to quaternion tensors and define quaternion KA (QKA), which is a helpful pretreatment step for QTT-rank based optimization problems. The details can be founded in Section V. To summarize, the main contributions of this paper are listed as follows:

- The QTT decomposition is first presented, and based on it the QTT-rank is naturally defined, which are the generalizations of their counterparts in the real number field.
- A general and flexible transform framework for quaternion tensors is defined, which can reveal the essential sparsity of visual data.
- Combining both the global low-QTT-rank and local sparse priors of the quaternion tensor, we propose a novel LRQTC model. Then, the model is optimized by applying the quaternion-based alternating direction method of multipliers (ADMM) algorithm.
- The QKA is defined for QTT-rank minimization approaches to handle color images and better handle color videos. Extensive experiments are conducted to demonstrate the effectiveness and superiority of the proposed method for inpainting problems of color images and color videos.

The remainder of this paper is organized as follows. Section II introduces some main notations and needed basic knowledge of quaternions. Section III presents the QTT decomposition and the QTT-rank. Section IV gives the proposed LRQCT model and the solving algorithm. A quaternion tensor augmentation technique, *i.e.*, QKA is introduced in Section V. Section VI provides extensive experiments to illustrate the performance of the proposed method. Finally, some conclusions are drawn in Section VII.

## II. PRELIMINARY

In this section, we list some main notations and introduce some needed basic knowledge of quaternions.

### A. Notations

In this paper,  $\mathbb{R}$ ,  $\mathbb{C}$ , and  $\mathbb{H}$  respectively denote the real space, complex space, and quaternion space. A scalar, a vector, a matrix, and a tensor are written as  $a$ ,  $\mathbf{a}$ ,  $\mathbf{A}$ , and  $\mathcal{A}$  respectively.  $\dot{a}$ ,  $\dot{\mathbf{a}}$ ,  $\dot{\mathbf{A}}$ , and  $\dot{\mathcal{A}}$  respectively represent a quaternion scalar, a quaternion vector, a quaternion matrix, and a quaternion tensor.  $(\cdot)^*$ ,  $(\cdot)^{-1}$ , and  $(\cdot)^H$  denote the conjugation, inverse, and conjugate transpose, respectively.  $|\cdot|$ ,  $\|\cdot\|_F$ ,  $\|\cdot\|_*$ ,  $\|\cdot\|_{w,*}$ , and  $\|\cdot\|_1$  are respectively the modulus, Frobenius norm, nuclear norm, weighted nuclear norm, and  $l_1$ -norm.  $\mathbf{X}_{(n)}$  and  $\mathbf{X}_{[n]}$  respectively denote mode- $n$  unfolding and mode- $n$  canonical unfolding of quaternion tensor  $\dot{\mathcal{X}}$ .  $\times_n$ ,  $\otimes$ , and  $\langle \cdot, \cdot \rangle$  are respectively the  $n$ -mode product, the Kronecker product, and the inner product.

### B. Basic Knowledge of Quaternions

Preliminaries of quaternions (including quaternion matrices and quaternion tensors) can be seen in Appendix A.

## III. QTT DECOMPOSITION AND QTT-RANK

As a generalization of the real-valued TT decomposition in [7], we define the following QTT decomposition:

**Definition 1.** (*QTT Decomposition*) Given an  $N$ -th order quaternion tensor  $\dot{\mathcal{X}} \in \mathbb{H}^{I_1 \times I_2 \times \dots \times I_N}$ , the QTT decomposition models each entry of  $\mathcal{X}$  by a series of quaternion matrix products as

$$\dot{x}_{i_1, i_2, \dots, i_N} = \dot{\mathcal{G}}_1(:, i_1, :) \dot{\mathcal{G}}_2(:, i_2, :) \dots \dot{\mathcal{G}}_N(:, i_N, :), \quad (7)$$

where  $\dot{\mathcal{G}}_n \in \mathbb{H}^{r_{n-1} \times I_n \times r_n}$ ,  $n = 1, 2, \dots, N$  with  $r_0 = r_N = 1$  are third-order quaternion tensors called the **cores** of  $\dot{\mathcal{X}}$  and  $(r_1, r_2, \dots, r_{N-1})$  is a vector closely related to the QTT-rank defined below. The graphical of QTT decomposition can be seen in Figure 1.

**Remark 1.** In the index form the QTT decomposition (7) can be written as

$$\dot{x}_{i_1, i_2, \dots, i_N} = \sum_{l_1, l_2, \dots, l_{N-1}=1}^{r_1, r_2, \dots, r_{N-1}} \dot{\mathcal{G}}_1(1, i_1, l_1) \dot{\mathcal{G}}_2(l_1, i_2, l_2) \dots \dot{\mathcal{G}}_N(l_{N-1}, i_N, 1). \quad (8)$$

In the following, we show that the QTT decomposition of a quaternion tensor  $\dot{\mathcal{X}} \in \mathbb{H}^{I_1 \times I_2 \times \dots \times I_N}$  can be derived recursively.

Firstly, treating the multi-index  $(i_2, \dots, i_N)$  as a single index, then we have a following usual quaternion matrix decomposition:

$$\dot{x}_{i_1, i_2, \dots, i_N} = \sum_{l_1=1}^{r_1} \dot{\mathcal{G}}_1(1, i_1, l_1) \dot{\mathcal{H}}_1(l_1, i_2, \dots, i_N). \quad (9)$$

Next, for quaternion tensor  $\dot{\mathcal{H}}_1$ , the indices  $(l_1, i_2)$  are separated from the rest, we also have a following usual quaternion matrix decomposition:

$$\dot{\mathcal{H}}_1(l_1, i_2, \dots, i_N) = \sum_{l_2=1}^{r_2} \dot{\mathcal{G}}_2(l_1, i_2, l_2) \dot{\mathcal{H}}_2(l_2, i_3, \dots, i_N). \quad (10)$$

Thus,

$$\begin{aligned} \dot{x}_{i_1, i_2, \dots, i_N} &= \sum_{l_1, l_2=1}^{r_1, r_2} \dot{\mathcal{G}}_1(1, i_1, l_1) \dot{\mathcal{G}}_2(l_1, i_2, l_2) \dot{\mathcal{H}}_2(l_2, i_3, \dots, i_N). \end{aligned}$$

Proceeding in the above way, after  $N$  steps, one can obtain a decomposition of the form (8).

**Remark 2.** From (7), one can easily find that the QTT decomposition of a quaternion tensor  $\dot{\mathcal{X}} \in \mathbb{H}^{I_1 \times I_2 \times \dots \times I_N}$  is not unique: we can insert the identity  $\dot{\mathbf{Q}}\dot{\mathbf{Q}}^{-1}$  between any two quaternion matrices in the series to obtain another decomposition.

**Remark 3.** Denote  $I = \max I_n$  and  $r = \max r_n$ , the number of parameters in the QTT decomposition (7) is upper bounded by  $NIr^2$ . To constitute a great reduction compared to storing  $\prod_{i=1}^N I_i$  entries in  $\mathcal{X}$  explicitly, we tend to choose the  $r_1, r_2, \dots, r_{N-1}$  as small as possible.

In the following, we first define another matricization operation for a quaternion tensor  $\dot{\mathcal{X}} \in \mathbb{H}^{I_1 \times I_2 \times \dots \times I_N}$  and then give an important theorem. They are the direct source of the QTT-rank definition.

**Definition 2.** (*Mode- $n$  canonical unfolding*) Mode- $n$  canonical unfolding of an  $N$ -th order quaternion tensor  $\dot{\mathcal{X}} \in \mathbb{H}^{I_1 \times I_2 \times \dots \times I_N}$  is defined as

$$\dot{\mathbf{X}}_{[n]} \in \mathbb{H}^{\prod_{j=1}^n I_j \times \prod_{j=n+1}^N I_j}, \quad (11)$$

within each dimension of the matrix  $\dot{\mathbf{X}}_{[n]}$ , the indices are ordered lexicographically, which is the same as calling Matlab's "reshape" function on a multidimensional array with the specified target dimension, i.e.,

$$\begin{aligned} \dot{\mathbf{X}}_{[n]} &= \text{reshape}(\dot{\mathcal{X}}, \prod_{j=1}^n I_j, \prod_{j=n+1}^N I_j) \\ &:= \text{unfold}_{[n]}(\dot{\mathcal{X}}). \end{aligned}$$

Conversely, the mode- $n$  canonical quaternion matrix  $\dot{\mathbf{X}}_{[n]}$  can be transformed back to the quaternion tensor  $\dot{\mathcal{X}}$  by

$$\begin{aligned} \dot{\mathcal{X}} &= \text{reshape}(\dot{\mathbf{X}}_{[n]}, I_1, I_2, \dots, I_N) \\ &:= \text{fold}_{[n]}(\dot{\mathbf{X}}_{[n]}). \end{aligned}$$

Compared with the Mode- $n$  unfolding operation in the Definition 7, the Mode- $n$  canonical unfolding is a well-balanced matricization characterizing the correlation between the first  $n$  and the rest  $N - n$  dimensions of  $\dot{\mathcal{X}}$ .

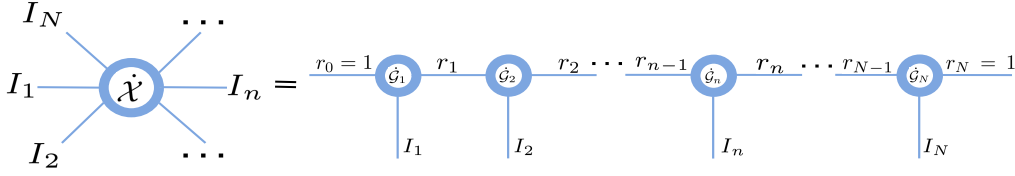


Fig. 1: The graphical of QTT decomposition.

**Theorem 1.** For an  $N$ -th order quaternion tensor  $\dot{\mathcal{X}} \in \mathbb{H}^{I_1 \times I_2 \times \dots \times I_N}$  with a QTT decomposition (7), it necessarily holds that

$$r_n \geq \text{rank}(\dot{\mathbf{X}}_{[n]}), \quad n = 1, 2, \dots, N-1, \quad (12)$$

and it is furthermore possible to obtain a QTT decomposition such that equality holds.

The proof of Theorem 1 can be founded in Appendix B. As described in Remark 3 that we tend to choose the  $r_1, r_2, \dots, r_{N-1}$  as small as possible. Theorem 1 tells us that  $\text{rank}(\dot{\mathbf{X}}_{[n]})$  is the lower bound of  $r_n$  and furthermore  $\text{rank}(\dot{\mathbf{X}}_{[n]})$  is an admissible choice for  $r_n$  with  $n = 1, 2, \dots, N-1$ . Therefore,  $\text{rank}(\dot{\mathbf{X}}_{[1]}), \text{rank}(\dot{\mathbf{X}}_{[2]}), \dots, \text{rank}(\dot{\mathbf{X}}_{[N-1]})$  are of interest to us, for which we give the following definition of QTT-rank.

**Definition 3.** (QTT-rank) QTT-rank of an  $N$ -th order quaternion tensor  $\dot{\mathcal{X}} \in \mathbb{H}^{I_1 \times I_2 \times \dots \times I_N}$  is defined as

$$\text{rank}_{\text{QTT}}(\dot{\mathcal{X}}) = (\text{rank}(\dot{\mathbf{X}}_{[1]}), \dots, \text{rank}(\dot{\mathbf{X}}_{[N-1]})). \quad (13)$$

One can see that  $\text{rank}(\dot{\mathbf{X}}_{[n]})(n = 1, 2, \dots, N-1)$  contains correlations between permutations of all modes of  $\dot{\mathcal{X}}$ , which gives an effective way to capture the global correlations of a quaternion tensor.

#### IV. LOW-RANK QUATERNION TENSOR COMPLETION MODEL AND SOLVING ALGORITHM

##### A. Sparse Regularization Method in a Transformed Domain

In the following, we define a general and flexible transform leading the quaternion tensor to a sparse space.

**Definition 4.** The transform  $\mathfrak{T}$  for an  $N$ -th order quaternion tensor  $\dot{\mathcal{X}} \in \mathbb{H}^{I_1 \times I_2 \times \dots \times I_N}$  is defined as

$$\mathfrak{T}(\dot{\mathcal{X}}) := \hat{\mathcal{X}} = \dot{\mathcal{X}} \times_1 \dot{\mathbf{T}}_1 \times_2 \dot{\mathbf{T}}_2 \times \dots \times_N \dot{\mathbf{T}}_N, \quad (14)$$

where  $\dot{\mathbf{T}}_n (n = 1, 2, \dots, N)$  are unitary quaternion transform matrices with appropriate size, e.g., quaternion discrete Fourier transforms (QDFT), quaternion

discrete Cosine transforms (QDCT), and any other appropriate transforms. The inverse transform of  $\mathfrak{T}$  is directly defined as

$$\mathfrak{T}^{-1}(\hat{\mathcal{X}}) := \dot{\mathcal{X}} = \hat{\mathcal{X}} \times_1 \dot{\mathbf{T}}_1^{-1} \times_2 \dot{\mathbf{T}}_2^{-1} \times \dots \times_N \dot{\mathbf{T}}_N^{-1}. \quad (15)$$

**Remark 4.** The defined  $\mathfrak{T}(\dot{\mathcal{X}})$  is a general and flexible framework. Firstly,  $\dot{\mathbf{T}}_n (n = 1, 2, \dots, N)$  in (14) can be any appropriate transforms including but not limited to QDFT, QDCT, quaternion discrete Z transforms (QDZT), quaternion discrete Walsh-Hadamard transform (QDWHT). Furthermore, in some specific applications,  $\dot{\mathbf{T}}_n (n = 1, 2, \dots, N)$  in (14) can be a mixture of different types of transforms. Figure 2(c) gives several examples of the defined transform  $\mathfrak{T}$  on a given quaternion tensor generated by the color image “lena”. One can find that for different kinds of transforms the defined transform  $\mathfrak{T}$  do lead to a sparse space (the modulus of the vast majority of entries of the quaternion tensor in transformed domains are very close to zero).

**Remark 5.** The above mentioned QDFT, QDCT, QDZT, and QDWHT are quaternion versions of their traditional counterparts, i.e., DFT [19], DCT [20], DZT [21], and DWHT [22]. In Appendix C, we give a general and simple way to transform these traditional transforms into quaternion versions by using the Cayley-Dickson form of the quaternion matrix.

##### B. Proposed Model

Based on the defined QTT-rank and the sparse regularization method in a transformed domain, we propose the following LRQTC model:

$$\begin{aligned} \min_{\dot{\mathcal{X}}} \quad & \text{rank}_{\text{QTT}}(\dot{\mathcal{X}}) + \lambda \|\mathfrak{T}(\dot{\mathcal{X}})\|_1 \\ \text{s.t.} \quad & P_{\Omega}(\dot{\mathcal{X}}) = P_{\Omega}(\dot{\mathcal{J}}), \end{aligned} \quad (16)$$

where  $\lambda$  is a nonnegative parameter,  $\dot{\mathcal{X}} \in \mathbb{H}^{I_1 \times I_2 \times \dots \times I_N}$  is a completed output  $N$ -th order quaternion tensor,  $\dot{\mathcal{J}} \in \mathbb{H}^{I_1 \times I_2 \times \dots \times I_N}$  is the observed  $N$ -th order quaternion tensor, and  $P_{\Omega}(\cdot)$  is the projection operator on  $\Omega$  which is the index of observed entries. In order for (16)



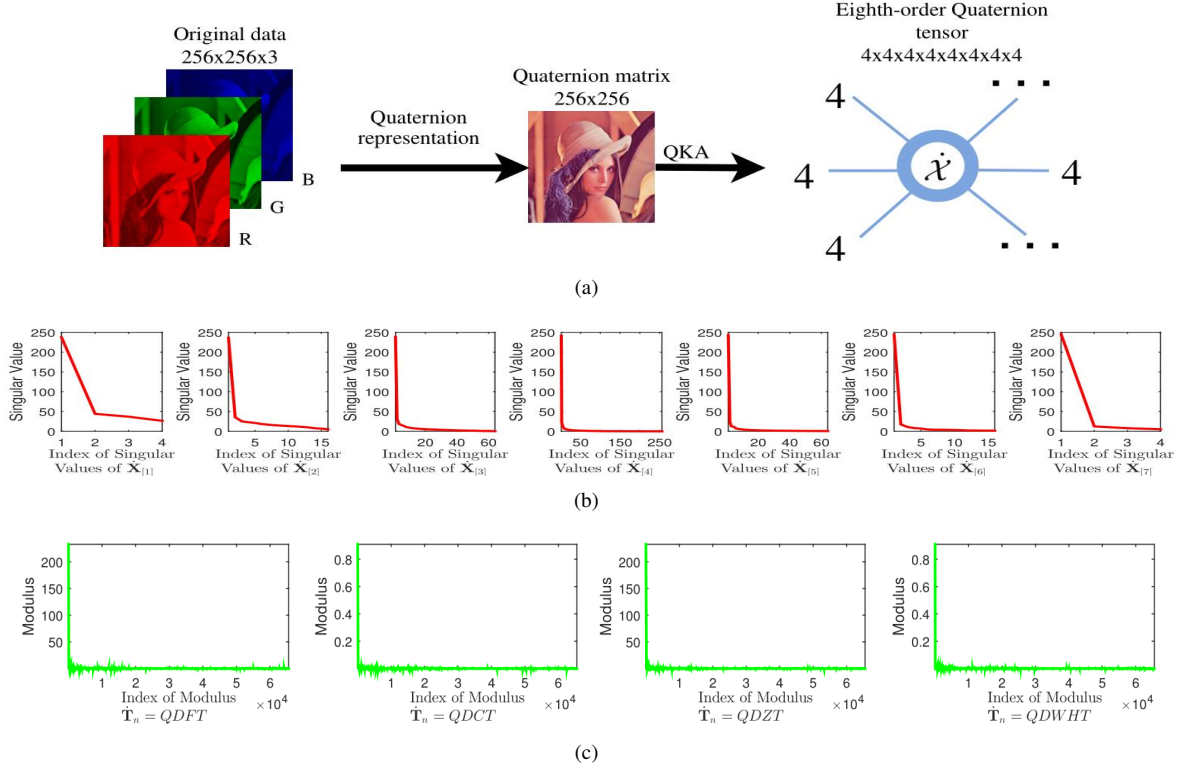


Fig. 2: (a) shows the process of a color image to higher-order quaternion tensor; (b) shows the low-QTT-rankness of the quaternion tensor generated by QKA; (c) shows the sparsity of the quaternion tensor in four transformed domains.

to be solved, we first use an effective non-convex surrogate (QWNN) to replace the QTT-rank function, then we use the variable-splitting technique and introduce auxiliary quaternion variables  $\dot{\mathcal{M}}_k \in \mathbb{H}^{I_1 \times I_2 \times \dots \times I_N}$  and  $\dot{\mathcal{E}}_k \in \mathbb{H}^{I_1 \times I_2 \times \dots \times I_N}$ , ( $k = 1, 2, \dots, N-1$ ) in (16). Consequently, (16) is finally transformed into the following solvable model:

$$\begin{aligned}
 & \min_{\dot{\mathcal{X}}, \dot{\mathcal{M}}_k, \dot{\mathcal{E}}_k} \sum_{k=1}^{N-1} \alpha_k \|\dot{\mathcal{M}}_{k[k]}\|_{w,*} + \lambda_k \|\dot{\mathcal{E}}_k\|_1 \\
 & \text{s.t. } P_\Omega(\dot{\mathcal{X}}) = P_\Omega(\dot{\mathcal{T}}) \\
 & \quad \dot{\mathcal{X}} = \dot{\mathcal{M}}_k, \quad k = 1, 2, \dots, N-1, \\
 & \quad \mathfrak{T}(\dot{\mathcal{X}}) = \dot{\mathcal{E}}_k, \quad k = 1, 2, \dots, N-1,
 \end{aligned} \tag{17}$$

where  $\alpha_k$  and  $\lambda_k$  for  $k = 1, 2, \dots, N-1$  are nonnegative parameters.

### C. Solving Algorithm

Based on the ADMM framework in the quaternion domain [23], the augmented Lagrangian function of (17)

is defined as

$$\begin{aligned}
 & \mathcal{L}_\mu(\dot{\mathcal{X}}, \{\dot{\mathcal{M}}_k\}_{k=1}^{N-1}, \{\dot{\mathcal{E}}_k\}_{k=1}^{N-1}, \{\dot{\mathcal{Y}}_{1k}\}_{k=1}^{N-1}, \{\dot{\mathcal{Y}}_{2k}\}_{k=1}^{N-1}) \\
 & = \sum_{k=1}^{N-1} \alpha_k \|\dot{\mathcal{M}}_{k[k]}\|_{w,*} + \lambda_k \|\dot{\mathcal{E}}_k\|_1 \\
 & \quad + \Re(\langle \dot{\mathcal{Y}}_{1k}, \dot{\mathcal{X}} - \dot{\mathcal{M}}_k \rangle) + \frac{\mu}{2} \|\dot{\mathcal{X}} - \dot{\mathcal{M}}_k\|_F^2 \\
 & \quad + \Re(\langle \dot{\mathcal{Y}}_{2k}, \mathfrak{T}(\dot{\mathcal{X}}) - \dot{\mathcal{E}}_k \rangle) + \frac{\mu}{2} \|\mathfrak{T}(\dot{\mathcal{X}}) - \dot{\mathcal{E}}_k\|_F^2,
 \end{aligned} \tag{18}$$

where  $\dot{\mathcal{Y}}_{1k} \in \mathbb{H}^{I_1 \times I_2 \times \dots \times I_N}$  and  $\dot{\mathcal{Y}}_{2k} \in \mathbb{H}^{I_1 \times I_2 \times \dots \times I_N}$  for  $k = 1, 2, \dots, N-1$  are Lagrange multipliers,  $\mu > 0$  is the penalty parameter. Then, we use the following

iterative scheme to solve the problem (18):

$$\left\{ \begin{array}{l} \dot{\mathcal{X}}^{(\tau+1)} = \arg \min_{P_{\Omega}(\dot{\mathcal{X}})=P_{\Omega}(\dot{\mathcal{T}})} \mathcal{L}_{\mu^{(\tau)}} \left( \dot{\mathcal{X}}, \{\dot{\mathcal{M}}_k^{(\tau)}\}_{k=1}^{N-1}, \right. \\ \quad \left. \{\dot{\mathcal{E}}_k^{(\tau)}\}_{k=1}^{N-1}, \{\dot{\mathcal{Y}}_{1k}^{(\tau)}\}_{k=1}^{N-1}, \{\dot{\mathcal{Y}}_{2k}^{(\tau)}\}_{k=1}^{N-1} \right), \\ \{\dot{\mathcal{M}}_k^{(\tau+1)}\}_{k=1}^{N-1} = \arg \min_{\{\dot{\mathcal{M}}_k\}_{k=1}^{N-1}} \mathcal{L}_{\mu^{(\tau)}} \left( \dot{\mathcal{X}}^{(\tau+1)}, \{\dot{\mathcal{M}}_k\}_{k=1}^{N-1}, \right. \\ \quad \left. \{\dot{\mathcal{E}}_k^{(\tau)}\}_{k=1}^{N-1}, \{\dot{\mathcal{Y}}_{1k}^{(\tau)}\}_{k=1}^{N-1}, \{\dot{\mathcal{Y}}_{2k}^{(\tau)}\}_{k=1}^{N-1} \right), \\ \{\dot{\mathcal{E}}_k^{(\tau+1)}\}_{k=1}^{N-1} = \arg \min_{\{\dot{\mathcal{E}}_k\}_{k=1}^{N-1}} \mathcal{L}_{\mu^{(\tau)}} \left( \dot{\mathcal{X}}^{(\tau+1)}, \{\dot{\mathcal{M}}_k^{(\tau+1)}\}_{k=1}^{N-1}, \right. \\ \quad \left. \{\dot{\mathcal{E}}_k\}_{k=1}^{N-1}, \{\dot{\mathcal{Y}}_{1k}^{(\tau)}\}_{k=1}^{N-1}, \{\dot{\mathcal{Y}}_{2k}^{(\tau)}\}_{k=1}^{N-1} \right), \\ \{\dot{\mathcal{Y}}_{1k}^{(\tau+1)}\}_{k=1}^{N-1} = \{\dot{\mathcal{Y}}_{1k}^{(\tau)}\}_{k=1}^{N-1} + \mu^{(\tau)} \left( \dot{\mathcal{X}}^{(\tau+1)} - \right. \\ \quad \left. \{\dot{\mathcal{M}}_k^{(\tau+1)}\}_{k=1}^{N-1} \right), \\ \{\dot{\mathcal{Y}}_{2k}^{(\tau+1)}\}_{k=1}^{N-1} = \{\dot{\mathcal{Y}}_{2k}^{(\tau)}\}_{k=1}^{N-1} + \mu^{(\tau)} \left( \mathfrak{T}(\dot{\mathcal{X}}^{(\tau+1)}) - \right. \\ \quad \left. \{\dot{\mathcal{E}}_k^{(\tau+1)}\}_{k=1}^{N-1} \right), \end{array} \right. \quad (19)$$

where  $\tau$  is the iteration index. Next, we provide the details for solving the subproblems in (19).

**Updating  $\dot{\mathcal{X}}$ :** In the  $(\tau + 1)$ -th iteration, fixing the other variables at their latest values,  $\dot{\mathcal{X}}^{(\tau+1)}$  is the optimal solution of the following problem:

$$\begin{aligned} \dot{\mathcal{X}}^{(\tau+1)} &= \arg \min_{P_{\Omega}(\dot{\mathcal{X}})=P_{\Omega}(\dot{\mathcal{T}})} \sum_{k=1}^{N-1} \Re(\langle \dot{\mathcal{Y}}_{1k}^{(\tau)}, \dot{\mathcal{X}} - \dot{\mathcal{M}}_k^{(\tau)} \rangle) \\ &\quad + \frac{\mu^{(\tau)}}{2} \|\dot{\mathcal{X}} - \dot{\mathcal{M}}_k^{(\tau)}\|_F^2 + \Re(\langle \dot{\mathcal{Y}}_{2k}^{(\tau)}, \mathfrak{T}(\dot{\mathcal{X}}) - \dot{\mathcal{E}}_k^{(\tau)} \rangle) \\ &\quad + \frac{\mu^{(\tau)}}{2} \|\mathfrak{T}(\dot{\mathcal{X}}) - \dot{\mathcal{E}}_k^{(\tau)}\|_F^2 \\ &= \arg \min_{P_{\Omega}(\dot{\mathcal{X}})=P_{\Omega}(\dot{\mathcal{T}})} \sum_{k=1}^{N-1} \frac{\mu^{(\tau)}}{2} \|\dot{\mathcal{X}} - \dot{\mathcal{M}}_k^{(\tau)} + \frac{\dot{\mathcal{Y}}_{1k}^{(\tau)}}{\mu^{(\tau)}}\|_F^2 \\ &\quad + \frac{\mu^{(\tau)}}{2} \|\mathfrak{T}(\dot{\mathcal{X}}) - \dot{\mathcal{E}}_k^{(\tau)} - \frac{\dot{\mathcal{Y}}_{2k}^{(\tau)}}{\mu^{(\tau)}}\|_F^2. \end{aligned} \quad (20)$$

Since  $\dot{\mathbf{T}}_n$  ( $n = 1, 2, \dots, N$ ) are unitary quaternion transform matrices in (14), we have  $\|\mathfrak{T}(\dot{\mathcal{X}}) - \dot{\mathcal{E}}_k^{(\tau)} - \frac{\dot{\mathcal{Y}}_{2k}^{(\tau)}}{\mu^{(\tau)}}\|_F^2 = \|\dot{\mathcal{X}} - \mathfrak{T}^{-1}(\dot{\mathcal{E}}_k^{(\tau)} + \frac{\dot{\mathcal{Y}}_{2k}^{(\tau)}}{\mu^{(\tau)}})\|_F^2$ , for  $k = 1, 2, \dots, N - 1$ . Hence, we can solve  $\dot{\mathcal{X}}$  through

$$\begin{aligned} \dot{\mathcal{X}}^{(\tau+1)} &= \arg \min_{P_{\Omega}(\dot{\mathcal{X}})=P_{\Omega}(\dot{\mathcal{T}})} \sum_{k=1}^{N-1} \mu^{(\tau)} \|\dot{\mathcal{X}} - \frac{1}{2}(\dot{\mathcal{M}}_k^{(\tau)} - \frac{\dot{\mathcal{Y}}_{1k}^{(\tau)}}{\mu^{(\tau)}}) \\ &\quad + \mathfrak{T}^{-1}(\dot{\mathcal{E}}_k^{(\tau)} + \frac{\dot{\mathcal{Y}}_{2k}^{(\tau)}}{\mu^{(\tau)}})\|_F^2 \\ &= P_{\Omega^c} \left( \frac{\sum_{k=1}^{N-1} (\dot{\mathcal{M}}_k^{(\tau)} - \frac{\dot{\mathcal{Y}}_{1k}^{(\tau)}}{\mu^{(\tau)}} + \mathfrak{T}^{-1}(\dot{\mathcal{E}}_k^{(\tau)} + \frac{\dot{\mathcal{Y}}_{2k}^{(\tau)}}{\mu^{(\tau)}}))}{2(N-1)} \right) \\ &\quad + P_{\Omega}(\dot{\mathcal{T}}). \end{aligned} \quad (21)$$

**Updating  $\{\dot{\mathcal{M}}_k\}_{k=1}^{N-1}$ :** In the  $(\tau+1)$ -th iteration, fixing the other variables at their latest values, each  $\dot{\mathcal{M}}_k^{(\tau+1)}$  is related to solving the following optimization problem:

$$\begin{aligned} \dot{\mathcal{M}}_k^{(\tau+1)} &= \arg \min_{\dot{\mathcal{M}}_k} \alpha_k \|\dot{\mathcal{M}}_{k[k]}\|_{w,*} \\ &\quad + \Re(\langle \dot{\mathcal{Y}}_{1k}^{(\tau)}, \dot{\mathcal{X}}^{(\tau+1)} - \dot{\mathcal{M}}_k \rangle) \\ &\quad + \frac{\mu^{(\tau)}}{2} \|\dot{\mathcal{X}}^{(\tau+1)} - \dot{\mathcal{M}}_k\|_F^2 \\ &= \arg \min_{\dot{\mathcal{M}}_k} \frac{\alpha_k}{\mu^{(\tau)}} \|\dot{\mathcal{M}}_{k[k]}\|_{w,*} \\ &\quad + \frac{1}{2} \|\dot{\mathcal{M}}_k - (\dot{\mathcal{X}}^{(\tau+1)} + \frac{\dot{\mathcal{Y}}_{1k}^{(\tau)}}{\mu^{(\tau)}})\|_F^2. \end{aligned} \quad (22)$$

Based on the equation that  $\|\dot{\mathcal{X}}\|_F = \|\dot{\mathcal{X}}_{[k]}\|_F$ , (22) can be rewritten as

$$\begin{aligned} \dot{\mathcal{M}}_k^{(\tau+1)} &= \arg \min_{\dot{\mathcal{M}}_k} \frac{\alpha_k}{\mu^{(\tau)}} \|\dot{\mathcal{M}}_{k[k]}\|_{w,*} \\ &\quad + \frac{1}{2} \|\dot{\mathcal{M}}_{k[k]} - (\dot{\mathcal{X}}_{[k]}^{(\tau+1)} + \frac{\dot{\mathcal{Y}}_{1k[k]}^{(\tau)}}{\mu^{(\tau)}})\|_F^2. \end{aligned} \quad (23)$$

Denote  $\dot{\mathbf{\Gamma}} := \dot{\mathcal{X}}_{[k]}^{(\tau+1)} + \frac{\dot{\mathcal{Y}}_{1k[k]}^{(\tau)}}{\mu^{(\tau)}}$  and let  $\dot{\mathbf{\Gamma}} = \dot{\mathbf{U}}_k \dot{\mathbf{\Sigma}}_k \dot{\mathbf{V}}_k^H$  be the QSVD of  $\dot{\mathbf{\Gamma}}$ , where

$$\dot{\mathbf{\Sigma}}_k = \begin{bmatrix} \text{diag}(\sigma_1(\dot{\mathbf{\Gamma}}), \dots, \sigma_s(\dot{\mathbf{\Gamma}})) \\ \mathbf{0} \end{bmatrix},$$

and  $\sigma_n(\dot{\mathbf{\Gamma}})$  is the  $n$ -th singular value of  $\dot{\mathbf{\Gamma}}$ ,  $s$  denotes the number of nonzero singular values of  $\dot{\mathbf{\Gamma}}$ . From [9], the problem (23) has the following closed-form solution:

$$\dot{\mathcal{M}}_k^{(\tau+1)} = \text{fold}_{[k]}(\dot{\mathbf{U}}_k \dot{\mathbf{\Sigma}}_k \dot{\mathbf{V}}_k^H), \quad (24)$$

where

$$\dot{\mathbf{\Sigma}}_k = \begin{bmatrix} \text{diag}(\sigma_1(\dot{\mathcal{M}}_{k[k]}^{(\tau+1)}), \dots, \sigma_s(\dot{\mathcal{M}}_{k[k]}^{(\tau+1)})) \\ \mathbf{0} \end{bmatrix},$$

and

$$\sigma_n(\dot{\mathcal{M}}_{k[k]}^{(\tau+1)}) = \begin{cases} 0, & \text{if } c_2 < 0 \\ \frac{c_1 + \sqrt{c_2}}{2}, & \text{if } c_2 \geq 0 \end{cases},$$

where  $c_1 = \sigma_n(\dot{\mathbf{\Gamma}}) - \epsilon$ ,  $c_2 = (\sigma_n(\dot{\mathbf{\Gamma}}) + \epsilon)^2 - 4C$ , and  $C$  is a compromising constant.

**Updating  $\{\dot{\mathcal{E}}_k\}_{k=1}^{N-1}$ :** In the  $(\tau + 1)$ -th iteration, fixing the other variables at their latest values, each  $\dot{\mathcal{E}}_k^{(\tau+1)}$  is

related to solving the following optimization problem:

$$\begin{aligned}
\dot{\mathcal{E}}_k^{(\tau+1)} &= \arg \min_{\dot{\mathcal{E}}_k} \lambda_k \|\dot{\mathcal{E}}_k\|_1 \\
&\quad + \Re(\langle \dot{\mathcal{Y}}_{2k}^{(\tau)}, \dot{\mathcal{E}}_k - \mathfrak{T}(\dot{\mathcal{X}}^{(\tau+1)}) \rangle) \\
&\quad + \frac{\mu^{(\tau)}}{2} \|\dot{\mathcal{E}}_k - \mathfrak{T}(\dot{\mathcal{X}}^{(\tau+1)})\|_F^2 \\
&= \arg \min_{\dot{\mathcal{E}}_k} \frac{\lambda_k}{\mu^{(\tau)}} \|\dot{\mathcal{E}}_k\|_1 \\
&\quad + \frac{1}{2} \|\dot{\mathcal{E}}_k - (\mathfrak{T}(\dot{\mathcal{X}}^{(\tau+1)}) - \frac{\dot{\mathcal{Y}}_{2k}^{(\tau)}}{\mu^{(\tau)}})\|_F^2 \\
&= \text{shinkQ}(\mathfrak{T}(\dot{\mathcal{X}}^{(\tau+1)}) - \frac{\dot{\mathcal{Y}}_{2k}^{(\tau)}}{\mu^{(\tau)}}, \frac{\lambda_k}{\mu^{(\tau)}}),
\end{aligned} \tag{25}$$

where, for any quaternion matrix  $\dot{\mathbf{X}} = [\dot{x}_{mn}] \in \mathbb{H}^{M \times N}$  and  $\gamma > 0$ ,  $\text{shinkQ}(\dot{\mathbf{X}}, \gamma)$  is defined as [24]

$$\text{shinkQ}(\dot{\mathbf{X}}, \gamma) = \text{signQ}(\dot{x}_{mn}) \max(|\dot{x}_{mn}| - \gamma, 0),$$

and

$$\text{signQ}(\dot{x}_{mn}) = \begin{cases} \frac{\dot{x}_{mn}}{|\dot{x}_{mn}|}, & \text{if } |\dot{x}_{mn}| \neq 0, \\ 0, & \text{otherwise.} \end{cases}$$

**Updating**  $\{\dot{\mathcal{Y}}_{1k}\}_{k=1}^{N-1}$ ,  $\{\dot{\mathcal{Y}}_{2k}\}_{k=1}^{N-1}$ , and  $\mu$ : In the  $(\tau + 1)$ -th iteration, fixing the other variables at their latest values, each  $\dot{\mathcal{Y}}_{1k}^{(\tau+1)}$ , each  $\dot{\mathcal{Y}}_{2k}^{(\tau+1)}$ , and  $\mu^{(\tau+1)}$  are respectively updated by:

$$\dot{\mathcal{Y}}_{1k}^{(\tau+1)} = \dot{\mathcal{Y}}_{1k}^{(\tau)} + \mu^{(\tau)} (\dot{\mathcal{X}}^{(\tau+1)} - \dot{\mathcal{M}}_k^{(\tau+1)}), \tag{26}$$

$$\dot{\mathcal{Y}}_{2k}^{(\tau+1)} = \dot{\mathcal{Y}}_{2k}^{(\tau)} + \mu^{(\tau)} (\mathfrak{T}(\dot{\mathcal{X}}^{(\tau+1)}) - \dot{\mathcal{E}}_k^{(\tau+1)}), \tag{27}$$

$$\mu^{(\tau+1)} = \min(\rho \mu^{(\tau)}, \mu_{\max}), \tag{28}$$

where  $\rho > 1$  is a constant parameter, and  $\mu_{\max}$  is the default maximum of  $\mu$ .

Finally, the algorithm of the **Quaternion Tensor Train rank minimization with Sparse Regularization in a Transformed Domain** for quaternion tensor completion (QTT-SRTD) is summarized in Table I.

## V. QUATERNION TENSOR AUGMENTATION

The ket augmentation (KA) [3] as a tensor augmentation technique, has been proved it explores the low-rank structure more obviously than the original one. Thus, KA is a helpful pretreatment step for TT rank-based optimization [25], [26].

In [3], the authors treat color images as third-order tensors whose third dimension is 3 and defined KA. In contrast, we treat color images as second-order quaternion tensors (quaternion matrices) and define quaternion KA (QKA) to represent a lower-order quaternion tensor by a higher-order one. For example, QKA reshapes a color image  $\dot{\mathbf{G}} \in \mathbb{H}^{M_1 \times M_2}$  ( $M_1 \times M_2 = 2^n \times 2^n$  is the number of pixels in the image) into an  $N$ -th

TABLE I: The calculation procedure of the proposed QTT-SRTD.

---

**Input:** The observed  $N$ -th order quaternion tensor  $\dot{\mathcal{T}} \in \mathbb{H}^{I_1 \times I_2 \times \dots \times I_N}$  with  $\Omega$  (the index of observed entries), unitary quaternion transform matrices  $\{\dot{\mathbf{T}}_n\}_{n=1}^N$ ,  $\{\lambda_k\}_{k=1}^{N-1}$ ,  $\{\alpha_k\}_{k=1}^{N-1}$ ,  $\mu_{\max}$  and  $\rho$ .

- 1: **Initialize**  $\{\dot{\mathcal{M}}_k^{(0)}\}_{k=1}^{N-1}$ ,  $\{\dot{\mathcal{E}}_k^{(0)}\}_{k=1}^{N-1}$ ,  $\{\dot{\mathcal{Y}}_{1k}^{(0)}\}_{k=1}^{N-1}$ ,  $\{\dot{\mathcal{Y}}_{2k}^{(0)}\}_{k=1}^{N-1}$ ,  $\mu^{(0)}$ , and  $\tau = 0$ .
- 2: **Repeat**
- 3: Update  $\dot{\mathcal{X}}^{(\tau+1)}$  via (21).
- 4: **for**  $k = 1$  to  $N - 1$  **do**
- 5:   Update  $\dot{\mathcal{M}}_k^{(\tau+1)}$  via (24);
- 6:   Update  $\dot{\mathcal{E}}_k^{(\tau+1)}$  via (25);
- 7:   Update  $\dot{\mathcal{Y}}_{1k}^{(\tau+1)}$  via (26);
- 8:   Update  $\dot{\mathcal{Y}}_{2k}^{(\tau+1)}$  via (27).
- 9: **end for**
- 10: Update  $\mu^{(\tau+1)}$  via (28).
- 11:  $\tau \leftarrow \tau + 1$ .
- 12: **Until**  $\frac{\|\dot{\mathcal{X}}^{(\tau+1)} - \dot{\mathcal{X}}^{(\tau)}\|_F}{\|\dot{\mathcal{T}}\|_F} < 10^{-5}$ .

---

**Output:** The recovered quaternion tensor  $\dot{\mathcal{X}}^{(\tau)}$ .

---

order quaternion tensor  $\dot{\mathcal{Q}} \in \mathbb{H}^{I_1 \times I_2 \times \dots \times I_N}$ , where  $M_1 M_2 = \prod_{j=1}^N I_j$ , and  $I_j$  represents a unique block structured addressing of the original color image. In the following, we give the details of the structured block addressing procedure of QKA.

For a color image  $\dot{\mathbf{G}} \in \mathbb{H}^{M_1 \times M_2}$ , we consider the initial smallest block (labeled as  $i_1$ ) with size  $2 \times 2$ , which can be represented as

$$\dot{\mathbf{G}}_{[2^1 \times 2^1]} = \sum_{i_1=1}^4 \dot{q}_{i_1} \mathbf{e}_{i_1}, \tag{29}$$

where  $\dot{q}_{i_1}$  is the color pixel value,  $\mathbf{e}_{i_1}$  is the orthonormal base, *i.e.*,  $\mathbf{e}_1 = (1, 0, 0, 0)$ ,  $\mathbf{e}_2 = (0, 1, 0, 0)$ ,  $\mathbf{e}_3 = (0, 0, 1, 0)$ , and  $\mathbf{e}_4 = (0, 0, 0, 1)$ . The value  $i_1 = 1$  can be understood as labeling the up-left color pixel,  $i_1 = 2$  as the up-right one,  $i_1 = 3$  as down-left one, and  $i_1 = 4$  as down-right one, *see* Figure 3 (left-hand side). We then consider a larger block (labeled as  $i_2$ ) with size  $4 \times 4$  made up of four inner sub-blocks as shown Figure 3 (right-hand side). The new block is represented by

$$\dot{\mathbf{G}}_{[2^2 \times 2^2]} = \sum_{i_2=1}^4 \sum_{i_1=1}^4 \dot{q}_{i_2 i_1} \mathbf{e}_{i_2} \otimes \mathbf{e}_{i_1}, \tag{30}$$

where  $\otimes$  denotes the Kronecker product. Generally, this block structure can be extended to a size of  $2^N \times 2^N$  step by step until it can present all the values of color pixels in the image. Finally, the color image can be cast into an  $N$ -th order quaternion tensor  $\dot{\mathcal{Q}} \in \mathbb{H}^{4 \times 4 \times \dots \times 4}$  containing all the color pixel values as follows:

$$\dot{\mathcal{Q}}_{[2^N \times 2^N]} = \sum_{i_N, \dots, i_2, i_1=1}^4 \dot{q}_{i_N \dots i_2 i_1} \mathbf{e}_{i_N} \otimes \dots \otimes \mathbf{e}_{i_2} \otimes \mathbf{e}_{i_1}. \tag{31}$$

**Remark 6.** The presentation (31) is suitable for color image processing as it preserves all the color pixel values and rearranges them in a higher-order quaternion tensor such that not only the QTT-rank minimization method can be well used to process color images, but also the richness of textures in the color image can be studied via the correlation between modes of the quaternion tensor. Figure 2(a) shows the process of converting a three-channel color image to an eighth-order quaternion tensor.

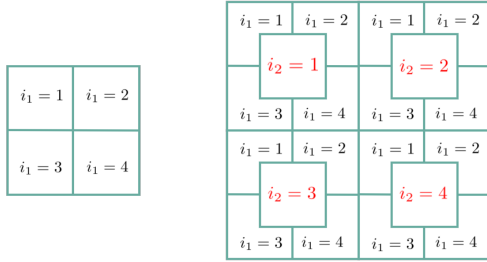


Fig. 3: The illustration of QKA casting a color image represented by a quaternion matrix to a higher-order quaternion tensor. The left-hand side is an example of a block with size  $2 \times 2$  represented by (29). The right-hand side is an example of a block with size  $2^2 \times 2^2$  represented by (30).

**Remark 7.** The defined QKA can also be used to rearrange a color video represented by a third-order quaternion tensor  $\dot{\mathcal{V}} \in \mathbb{H}^{C_1 \times C_2 \times F}$  (image row  $\times$  image column  $\times$  frame) in a higher-order quaternion tensor  $\dot{\mathcal{J}} \in \mathbb{H}^{I_1 \times I_2 \times \dots \times I_N \times F}$ , where  $C_1 C_2 = \prod_{j=1}^N I_j$ . The general form is given by

$$\begin{aligned} & \dot{\mathcal{V}}_{[2^N \times 2^N \times F]} \\ &= \sum_{i_N, \dots, i_1=1}^4 \sum_{f=1}^F \dot{i}_{i_N \dots i_1} \mathbf{e}_{i_N} \otimes \dots \otimes \mathbf{e}_{i_1} \otimes \mathbf{u}_f, \end{aligned} \quad (32)$$

where  $\mathbf{u}_f$  is also an orthonormal base defined as  $\mathbf{u}_1 = (1, 0, \dots, 0)$ ,  $\mathbf{u}_2 = (0, 1, \dots, 0)$ ,  $\dots$ ,  $\mathbf{u}_F = (0, 0, \dots, 1)$ . In addition, it should be noted that in (31) and (32),  $i_n = 1, \dots, c$ , where  $c > 1$  can be any appropriate value, i.e.,  $c = 4$  is not necessary.

## VI. NUMERICAL EXPERIMENTS

In this section, extensive experiments are conducted to demonstrate the effectiveness and superiority of the proposed QTT-SRTD for inpainting problems of color images and color videos. All the experiments are run in MATLAB 2014b under Windows 10 on a personal computer with a 1.60GHz CPU and 8GB memory.

### A. Color Image Inpainting

In this experiment, we apply the proposed QTT-SRTD to color image inpainting from incomplete entries.

**Compared methods:** We compare the proposed QTT-SRTD with several well-known methods including t-SVD [2], SiLRTC-TT [3], TMac-TT [3], LRQA-2 [11], LRQMC [13], and TQLNA [14].

**Parameter and initialization setting<sup>1</sup>:** For our proposed QTT-SRTD in Table I, we choose all quaternion transform matrices  $\{\dot{\mathbf{T}}_n\}_{n=1}^N$  as QDWHT<sup>2</sup>, all  $\{\lambda_k\}_{k=1}^{N-1}$  are seted as 0.01, all  $\{\alpha_k\}_{k=1}^{N-1}$  are seted as  $\frac{1}{N-1}$ ,  $\mu_{\max} = 10^6$ , and  $\rho = 1.08$ .  $\{\mathcal{M}_k^{(0)}\}_{k=1}^{N-1}$ ,  $\{\dot{\mathcal{E}}_k^{(0)}\}_{k=1}^{N-1}$ ,  $\{\dot{\mathcal{Y}}_{1k}^{(0)}\}_{k=1}^{N-1}$ , and  $\{\dot{\mathcal{Y}}_{2k}^{(0)}\}_{k=1}^{N-1}$ , are all simply initialized to random quaternion matrices.  $\mu^{(0)}$  is initialized to  $2.5 \times 10^{-3}$ . In addition, all compared methods are from the source codes and the parameter settings are based on the suggestions in the original papers.

**Test data and settings:** Numerical comparisons are implemented on eight common-used color images (including “baboon”, “house”, “airplane”, “peppers”, “sailboat”, “lena”, “panda”, and “barbara”, see Figure 4) with size  $256 \times 256$ . For the QTT-SRTD, the color images are transformed into eighth-order quaternion tensors with size  $4 \times 4 \times 4 \times 4 \times 4 \times 4 \times 4 \times 4$  by QKA. In addition, for random missing, we set four levels of sampling rates (SRs) which are SR = 10%, SR = 20%, SR = 30%, and SR = 40%. For structural missing, we use eight kinds of structural missing pixels, see the first column in Figure 8.

Table II lists the PSNR and SSIM values of different methods on the eight color images with four levels of sampling rates, and Figure 5 gives the average PSNR and SSIM values. It is observed that for different levels of sampling rates, the proposed QTT-SRTD achieves the highest PSNR and SSIM values. Figure 6 and Figure 7 visually display the recovered results by different methods for random missing with SR = 10% and SR = 40%. From Figure 6 and Figure 7, one can see that the recovered results by the proposed QTT-SRTD are visually better than those of the compared methods. From the zoom-in regions of recovered images, the proposed QTT-SRTD can keep more details and smoothness of images compared with other methods. Experimental results of eight kinds of structural missing pixels are given in Table III and Figure 8, from which

<sup>1</sup>All parameter choices and initialization settings are based on empirical and experimental results.

<sup>2</sup>One can try other transforms, but here we just use QDWHT without explanation based on the results of the experiment. The difference between different transforms in specific applications is not the focus of this paper.



Fig. 4: Original color images.

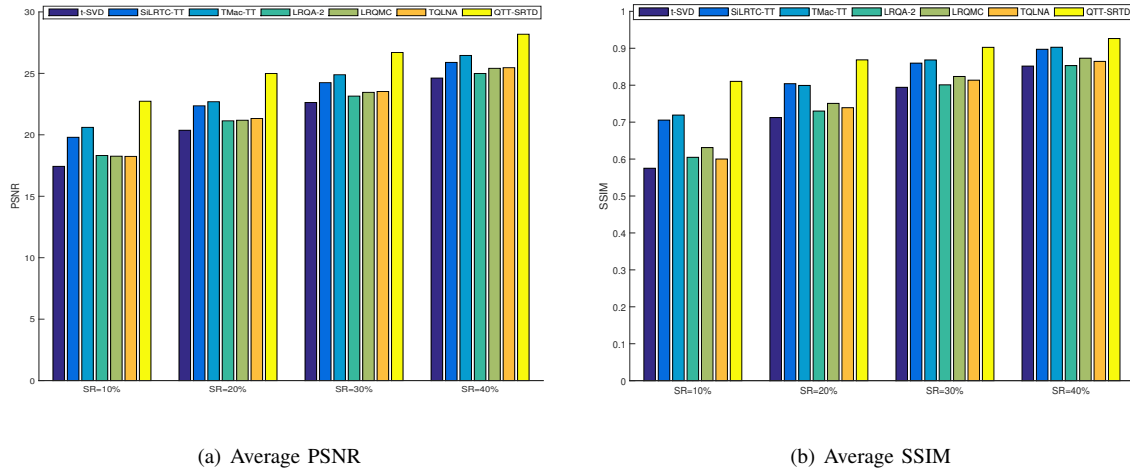


Fig. 5: Average PSNR and SSIM values of different methods on the eight color images with four levels of sampling rates.

one can find that the proposed QTT-SRTD achieves the highest PSNR and SSIM values and also better visually.

### B. Color Video Inpainting

In this experiment, we apply the proposed QTT-SRTD to color video inpainting from incomplete entries.

**Compared methods:** We compare the proposed QTT-SRTD with several well-known methods including t-SVD [2], SiLRTC-TT [3], TMac-TT [3], and LRC-QT [15].

**Parameter and initialization setting:** Same setting with color image inpainting.

**Test data and settings:** Numerical comparisons are implemented on two color videos<sup>3</sup> (including “Tempete”,

and “Foreman”, see Figure 9(a) with size  $256 \times 256 \times 20$ . For the QTT-SRTD, the color videos are transformed into fifth-order quaternion tensors with size  $16 \times 16 \times 16 \times 16 \times 20$  by QKA.

Figure 9 visually shows the recovered results of the 1st and 20th frames of “Tempete” and “Foreman” by different methods for random missing with  $SR = 20\%$ . Table IV gives the average PSNR and SSIM values of different methods on the two color videos with two levels of sampling rates ( $SR = 10\%$  and  $SR = 20\%$ ). We note that the proposed QTT-SRTD visually outperforms compared methods. The average PSNR and SSIM values achieved by the proposed QTT-SRTD are the highest.

<sup>3</sup><http://trace.eas.asu.edu/yuv/>

TABLE II: The PSNR and SSIM values of different methods on the eight color images with four levels of sampling rates (the format is PSNR/SSIM, and **bold** fonts denote the best performance).

| Methods: | t-SVD [2]    | SiLRTC-TT [3] | TMac-TT [3]  | LRQA-2 [11]  | LRQMC [13]   | TQLNA [14]   | <b>QTT-SRTD</b>     |
|----------|--------------|---------------|--------------|--------------|--------------|--------------|---------------------|
| Images:  | SR = 10%     |               |              |              |              |              |                     |
| baboon   | 17.325/0.505 | 18.484/0.563  | 19.242/0.579 | 17.941/0.527 | 18.065/0.546 | 18.075/0.537 | <b>20.445/0.656</b> |
| house    | 19.247/0.696 | 21.239/0.789  | 22.582/0.817 | 20.069/0.718 | 20.091/0.730 | 19.908/0.716 | <b>24.660/0.883</b> |
| airplane | 17.765/0.377 | 20.025/0.596  | 20.503/0.588 | 18.601/0.424 | 18.715/0.480 | 18.442/0.416 | <b>22.337/0.753</b> |
| peppers  | 15.993/0.718 | 18.894/0.842  | 20.416/0.871 | 17.111/0.761 | 16.206/0.740 | 17.145/0.764 | <b>22.815/0.920</b> |
| sailboat | 16.514/0.502 | 17.920/0.618  | 17.606/0.670 | 17.103/0.550 | 17.295/0.581 | 16.711/0.526 | <b>20.355/0.783</b> |
| lena     | 17.659/0.798 | 20.804/0.888  | 21.616/0.877 | 18.607/0.811 | 18.553/0.825 | 18.528/0.802 | <b>23.982/0.932</b> |
| panda    | 18.074/0.492 | 21.188/0.657  | 22.518/0.628 | 19.205/0.514 | 19.212/0.562 | 19.149/0.513 | <b>24.425/0.770</b> |
| barbara  | 16.894/0.513 | 19.834/0.691  | 20.373/0.723 | 17.917/0.533 | 17.947/0.585 | 17.996/0.527 | <b>22.840/0.786</b> |
| Images:  | SR = 20%     |               |              |              |              |              |                     |
| baboon   | 19.303/0.622 | 20.423/0.677  | 20.915/0.696 | 19.530/0.623 | 19.726/0.646 | 19.830/0.640 | <b>21.690/0.729</b> |
| house    | 22.492/0.827 | 23.954/0.871  | 23.788/0.856 | 23.193/0.836 | 23.320/0.849 | 23.335/0.843 | <b>27.507/0.932</b> |
| airplane | 20.441/0.555 | 22.185/0.739  | 22.024/0.721 | 21.014/0.580 | 21.160/0.629 | 21.114/0.592 | <b>24.632/0.839</b> |
| peppers  | 19.424/0.846 | 21.981/0.905  | 23.059/0.916 | 20.732/0.874 | 20.699/0.879 | 21.086/0.883 | <b>25.791/0.956</b> |
| sailboat | 18.858/0.663 | 20.218/0.762  | 21.100/0.794 | 19.472/0.693 | 19.570/0.716 | 19.567/0.699 | <b>22.602/0.858</b> |
| lena     | 20.859/0.876 | 23.594/0.927  | 23.442/0.914 | 21.698/0.886 | 21.901/0.897 | 21.804/0.889 | <b>26.200/0.955</b> |
| panda    | 21.397/0.639 | 23.901/0.761  | 23.774/0.691 | 22.307/0.657 | 22.373/0.690 | 22.505/0.669 | <b>26.220/0.825</b> |
| barbara  | 20.199/0.671 | 22.619/0.791  | 23.439/0.807 | 21.155/0.691 | 20.739/0.700 | 21.381/0.698 | <b>25.244/0.855</b> |
| Images:  | SR = 30%     |               |              |              |              |              |                     |
| baboon   | 20.657/0.703 | 21.656/0.749  | 21.801/0.751 | 20.685/0.695 | 21.279/0.727 | 20.878/0.705 | <b>22.684/0.784</b> |
| house    | 24.944/0.887 | 26.106/0.913  | 26.849/0.908 | 25.428/0.889 | 25.640/0.900 | 25.836/0.899 | <b>29.592/0.954</b> |
| airplane | 22.555/0.671 | 23.943/0.820  | 24.096/0.821 | 22.982/0.681 | 23.183/0.724 | 23.250/0.702 | <b>26.416/0.887</b> |
| peppers  | 22.287/0.908 | 24.293/0.939  | 25.458/0.951 | 23.330/0.923 | 23.671/0.930 | 23.976/0.934 | <b>27.941/0.973</b> |
| sailboat | 20.958/0.767 | 22.111/0.838  | 22.819/0.862 | 21.343/0.779 | 21.634/0.806 | 21.609/0.792 | <b>24.303/0.900</b> |
| lena     | 23.217/0.917 | 25.595/0.949  | 26.136/0.951 | 23.729/0.921 | 24.173/0.931 | 24.059/0.927 | <b>28.022/0.968</b> |
| panda    | 23.698/0.730 | 25.684/0.821  | 26.602/0.837 | 24.297/0.739 | 24.479/0.772 | 24.721/0.753 | <b>27.715/0.863</b> |
| barbara  | 22.737/0.771 | 24.560/0.849  | 25.338/0.866 | 23.403/0.781 | 23.584/0.799 | 23.885/0.797 | <b>26.902/0.891</b> |
| Images:  | SR = 40%     |               |              |              |              |              |                     |
| baboon   | 21.837/0.764 | 22.814/0.804  | 22.621/0.796 | 21.787/0.756 | 22.414/0.785 | 21.936/0.763 | <b>23.696/0.830</b> |
| house    | 27.360/0.929 | 27.995/0.940  | 28.944/0.941 | 27.744/0.929 | 28.140/0.939 | 28.403/0.938 | <b>31.329/0.968</b> |
| airplane | 24.501/0.761 | 25.634/0.871  | 26.184/0.878 | 24.754/0.757 | 24.992/0.798 | 25.208/0.781 | <b>28.071/0.917</b> |
| peppers  | 24.772/0.943 | 26.208/0.959  | 27.160/0.967 | 25.624/0.952 | 26.153/0.958 | 26.299/0.959 | <b>29.568/0.981</b> |
| sailboat | 22.782/0.837 | 23.795/0.888  | 24.176/0.900 | 23.099/0.844 | 23.321/0.861 | 23.472/0.855 | <b>25.850/0.928</b> |
| lena     | 25.221/0.943 | 27.291/0.964  | 27.726/0.965 | 25.624/0.945 | 26.126/0.953 | 26.061/0.950 | <b>29.563/0.977</b> |
| panda    | 25.653/0.799 | 27.187/0.863  | 28.168/0.878 | 25.985/0.799 | 26.387/0.829 | 26.484/0.814 | <b>28.987/0.892</b> |
| barbara  | 24.820/0.838 | 26.213/0.889  | 26.690/0.897 | 25.321/0.843 | 25.749/0.862 | 25.825/0.856 | <b>28.410/0.918</b> |

## VII. CONCLUSIONS

In this paper, the QTT decomposition is first proposed, and based on it the QTT-rank is naturally defined. In addition, a general and flexible transform framework is defined for utilizing the local sparse prior of the quaternion tensor. Combining both the global low-QTT-rank and local sparse priors of the quaternion tensor, a novel LRQTC model, *i.e.*, QTT-SRTD is proposed, which is optimized by ADMM algorithm. Furthermore, The QKA is defined for QTT-rank minimization ap-

proaches to handle color images and better handle color videos. Extensive experimental results are given to show the effectiveness and superiority of the proposed method for inpainting problems of color images and color videos. In the future, we would like to extend QTT-SRTD to other visual processing tasks, *e.g.*, image denoising.



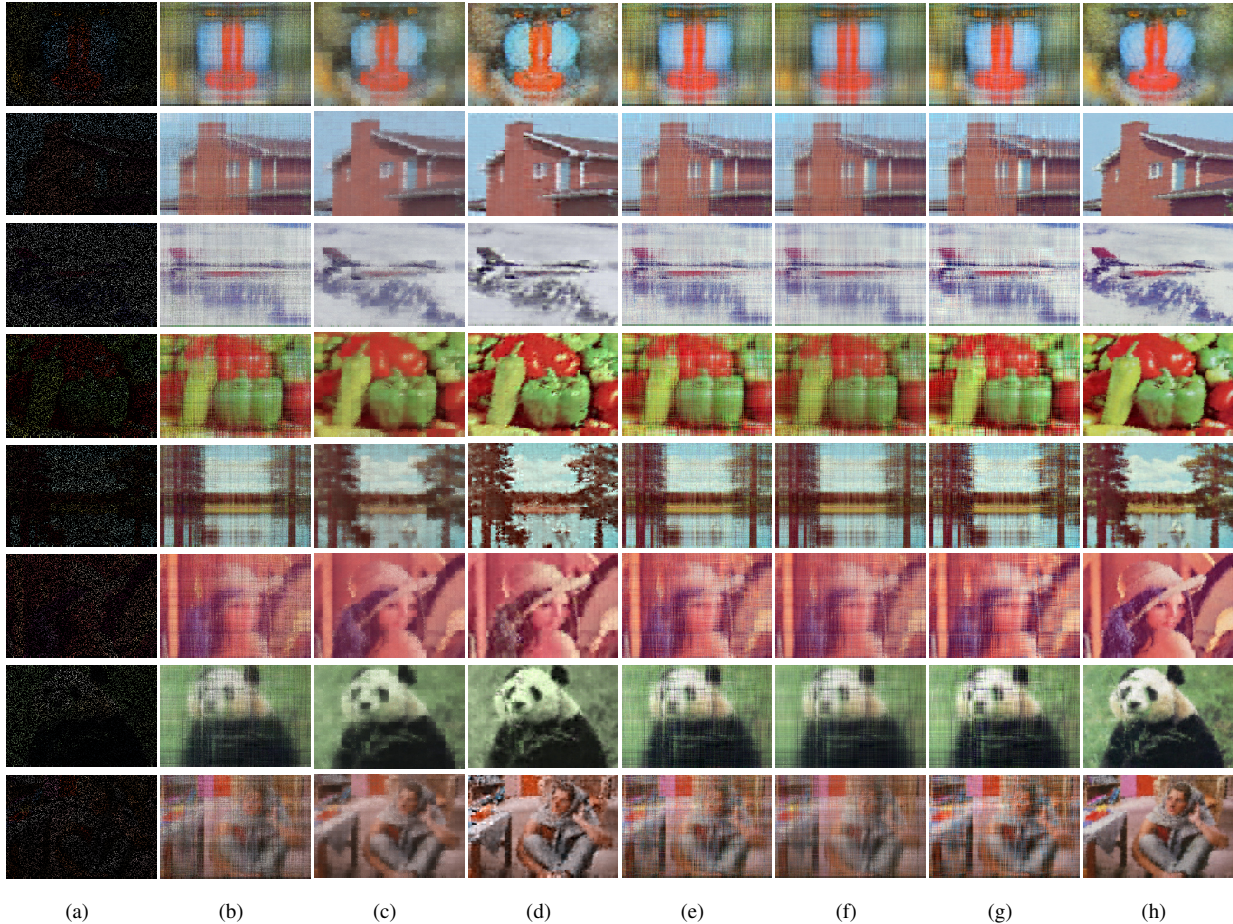


Fig. 6: Recovered color images for random missing with  $SR = 10\%$ . From left to right: the observed color images, the recovered results by t-SVD, SiLRTC-TT, TMac-TT, LRQA-2, LRQMC, TQLNA, and QTT-SRTD, respectively. From top to bottom: baboon, house, airplane, peppers, sailboat, lena, panda, and barbara.

TABLE III: The PSNR and SSIM values of different methods on the eight kinds of structural missing pixels (the format is PSNR/SSIM, and **bold** fonts denote the best performance).

| Methods: | t-SVD [2]    | SiLRTC-TT [3] | TMac-TT [3]  | LRQA-2 [11]  | LRQMC [13]   | TQLNA [14]   | <b>QTT-SRTD</b>     |
|----------|--------------|---------------|--------------|--------------|--------------|--------------|---------------------|
| Images:  | PSNR/SSIM    | PSNR/SSIM     | PSNR/SSIM    | PSNR/SSIM    | PSNR/SSIM    | PSNR/SSIM    | PSNR/SSIM           |
| baboon   | 29.848/0.963 | 30.459/0.968  | 30.268/0.967 | 29.258/0.954 | 29.829/0.962 | 29.426/0.959 | <b>31.080/0.971</b> |
| house    | 35.989/0.989 | 36.144/0.990  | 35.258/0.988 | 33.569/0.978 | 36.648/0.990 | 36.714/0.990 | <b>37.895/0.993</b> |
| airplane | 30.317/0.952 | 32.067/0.972  | 31.069/0.972 | 29.630/0.913 | 30.455/0.956 | 30.860/0.958 | <b>33.115/0.980</b> |
| peppers  | 32.517/0.992 | 34.933/0.995  | 33.596/0.994 | 32.297/0.991 | 32.512/0.993 | 31.780/0.992 | <b>36.733/0.997</b> |
| sailboat | 31.385/0.978 | 31.024/0.979  | 31.556/0.982 | 31.214/0.972 | 31.721/0.980 | 31.994/0.980 | <b>33.744/0.988</b> |
| lena     | 33.399/0.992 | 35.634/0.995  | 33.591/0.993 | 31.699/0.987 | 33.474/0.993 | 33.445/0.993 | <b>36.334/0.996</b> |
| panda    | 30.111/0.943 | 31.766/0.961  | 32.228/0.962 | 29.898/0.921 | 30.888/0.950 | 30.905/0.947 | <b>32.954/0.968</b> |
| barbara  | 30.763/0.971 | 31.518/0.977  | 30.614/0.973 | 30.730/0.957 | 30.957/0.971 | 31.531/0.971 | <b>33.377/0.980</b> |
| Aver.    | 31.791/0.973 | 32.943/0.980  | 32.273/0.979 | 31.037/0.959 | 32.061/0.974 | 32.082/0.974 | <b>34.404/0.984</b> |

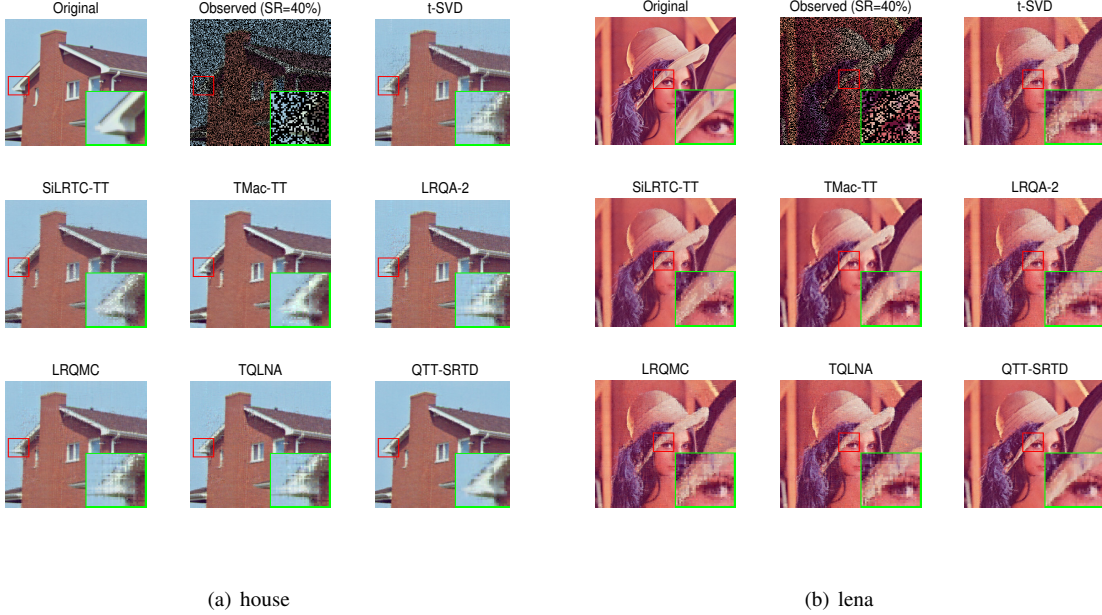


Fig. 7: Recovered two color images (house and lena) for random missing with SR = 40%.

TABLE IV: The PSNR and SSIM values (the average of 20 frames) of different methods on the two color videos with two levels of sampling rates (the format is PSNR/SSIM, and **bold** fonts denote the best performance).

| Methods: | t-SVD [2]    | SiLRTC-TT [3] | TMac-TT [3]  | LRC-QT [15]  | <b>QTT-SRTD</b>     |
|----------|--------------|---------------|--------------|--------------|---------------------|
| Videos:  | SR = 10%     |               |              |              |                     |
| Tempete  | 20.922/0.697 | 20.251/0.720  | 22.302/0.780 | 20.108/0.673 | <b>23.249/0.821</b> |
| Foreman  | 22.323/0.755 | 22.119/0.821  | 25.500/0.866 | 21.265/0.760 | <b>27.266/0.899</b> |
| Videos:  | SR = 20%     |               |              |              |                     |
| Tempete  | 23.229/0.802 | 22.425/0.820  | 23.683/0.836 | 21.842/0.747 | <b>25.283/0.878</b> |
| Foreman  | 25.020/0.840 | 24.993/0.891  | 26.850/0.901 | 24.053/0.843 | <b>29.960/0.936</b> |

#### APPENDIX A QUATERNIONS

Quaternion space  $\mathbb{H}$  was first introduced by W. Hamilton [27] in 1843, which is an extension of the complex space  $\mathbb{C}$ . A quaternion  $\dot{q} \in \mathbb{H}$  is given by

$$\dot{q} = q_0 + q_1i + q_2j + q_3k, \quad (33)$$

where  $q_l \in \mathbb{R}$  ( $l = 0, 1, 2, 3$ ), and  $i, j, k$  are imaginary units satisfying

$$\begin{cases} i^2 = j^2 = k^2 = ijk = -1, \\ ij = -ji = k, jk = -kj = i, ki = -ik = j. \end{cases} \quad (34)$$

If the real part  $q_0 = 0$ ,  $\dot{q}$  is called a pure quaternion. The addition and multiplication of quaternions are similar to complex numbers. It is worth noting that, unlike real and complex numbers, the multiplication of quaternions is not commutative, i.e., for two quaternions  $\dot{p} \in \mathbb{H}$  and  $\dot{q} \in$

$\mathbb{H}$ , in general,  $\dot{p}\dot{q} \neq \dot{q}\dot{p}$ . The conjugate and the modulus of a quaternion  $\dot{q}$  are, respectively, given by  $\dot{q}^* = q_0 - q_1i - q_2j - q_3k$  and  $|\dot{q}| = \sqrt{\dot{q}\dot{q}^*} = \sqrt{q_0^2 + q_1^2 + q_2^2 + q_3^2}$ .

Analogously, a quaternion matrix  $\dot{\mathbf{Q}} = (\dot{q}_{mn}) \in \mathbb{H}^{M \times N}$  is given by  $\dot{\mathbf{Q}} = \mathbf{Q}_0 + \mathbf{Q}_1i + \mathbf{Q}_2j + \mathbf{Q}_3k$ , where  $\mathbf{Q}_l \in \mathbb{R}^{M \times N}$  ( $l = 0, 1, 2, 3$ ). A quaternion matrix  $\dot{\mathbf{Q}}$  is called to be pure if  $\mathbf{Q}_0 = \mathbf{0}$ .

**Definition 5.** (Cayley-Dickson form [28]): For any quaternion matrix  $\dot{\mathbf{Q}} = \mathbf{Q}_0 + \mathbf{Q}_1i + \mathbf{Q}_2j + \mathbf{Q}_3k \in \mathbb{H}^{M \times N}$ , it can be represented as  $\dot{\mathbf{Q}} = \mathbf{Z}_1 + \mathbf{Z}_2j$ , where  $\mathbf{Z}_1 = \mathbf{Q}_0 + \mathbf{Q}_1i$  and  $\mathbf{Z}_2 = \mathbf{Q}_2 + \mathbf{Q}_3i$  are complex matrices.

**Theorem 2.** (Quaternion singular value decomposition (QSVD) [28]): For any quaternion matrix  $\dot{\mathbf{Q}} \in \mathbb{H}^{M \times N}$  with rank  $r$ , there exist unitary quaternion matrices  $\dot{\mathbf{U}} \in \mathbb{H}^{M \times M}$  and  $\dot{\mathbf{V}} \in \mathbb{H}^{N \times N}$  such that  $\dot{\mathbf{Q}} = \dot{\mathbf{U}} \begin{bmatrix} \Sigma_r & \mathbf{0} \\ \mathbf{0} & \mathbf{0} \end{bmatrix} \dot{\mathbf{V}}^H$ , where  $\Sigma_r = \text{diag}(\sigma_1, \dots, \sigma_r)$  is a real diagonal matrix with  $r$  positive entries  $\sigma_k$ , ( $k = 1, \dots, r$ ) on its diagonal, which are



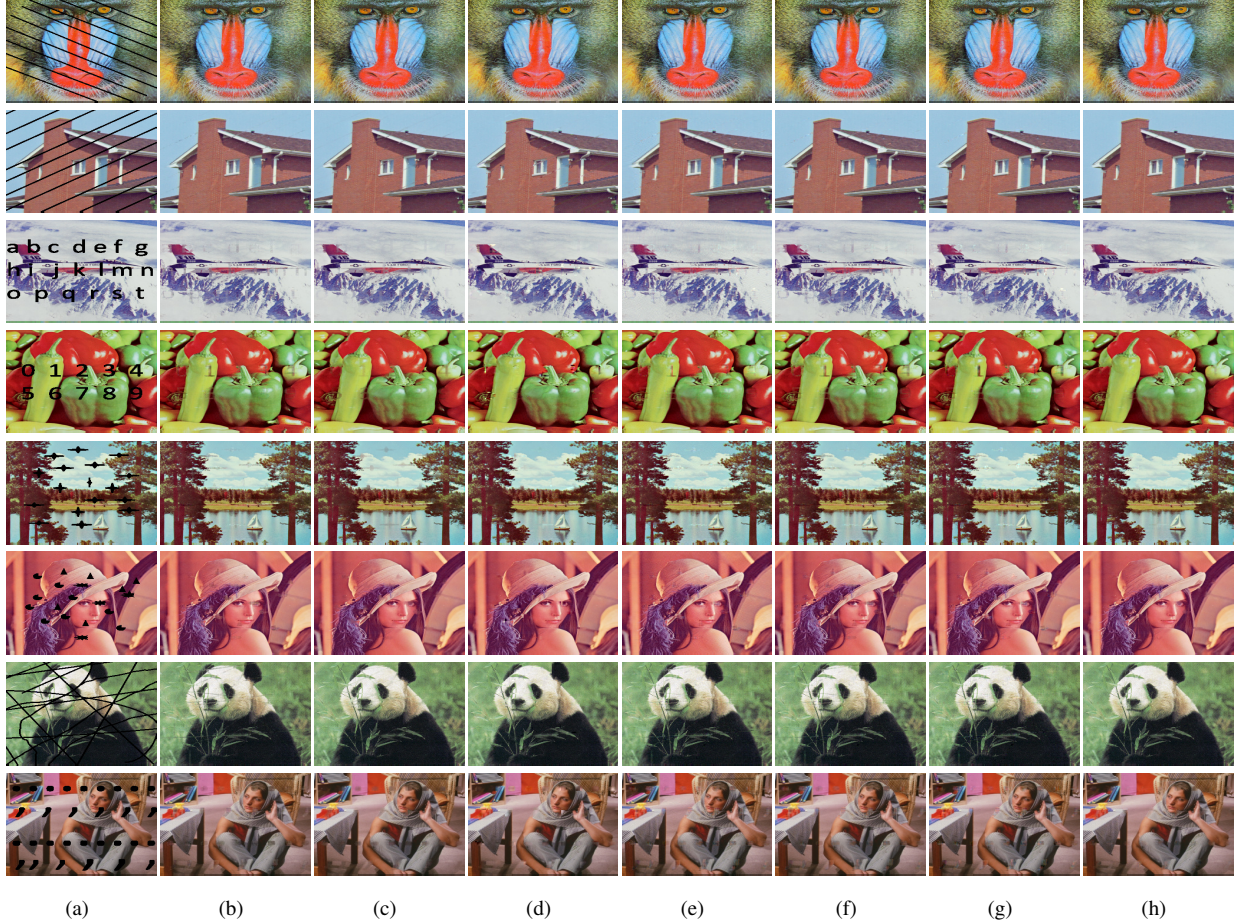


Fig. 8: Recovered color images for eight kinds of structural missing pixels. From left to right: the observed color images, the recovered results by t-SVD, SiLRTC-TT, TMac-TT, LRQA-2, LRQMC, TQLNA, and QTT-SRTD, respectively. From top to bottom: baboon, house, airplane, peppers, sailboat, lena, panda, and barbara. **The figure is viewed better in zoomed PDF.**

positive singular values of quaternion matrix  $\dot{\mathbf{Q}}$ .

The quaternion matrix Frobenius norm,  $l_1$ -norm, and quaternion nuclear norm are respectively given by  $\|\dot{\mathbf{Q}}\|_F = \sqrt{\sum_{m=1}^M \sum_{n=1}^N |\dot{q}_{mn}|^2}$ ,  $\|\dot{\mathbf{Q}}\|_1 = \sum_{m=1}^M \sum_{n=1}^N |\dot{q}_{mn}|$ , and  $\|\dot{\mathbf{Q}}\|_* = \sum_k \sigma_k$ .

**Definition 6.** (Quaternion tensor [15]) A multidimensional array or an  $N$ th-order tensor is named a quaternion tensor if its entries are quaternion numbers, i.e.,  $\mathcal{X} = (\dot{x}_{i_1 i_2 \dots i_N}) \in \mathbb{H}^{I_1 \times I_2 \times \dots \times I_N} = \mathcal{X}_0 + \mathcal{X}_1 i + \mathcal{X}_2 j + \mathcal{X}_3 k$ , where  $\mathcal{X}_l \in \mathbb{R}^{I_1 \times I_2 \times \dots \times I_N}$  ( $l = 0, 1, 2, 3$ ),  $\mathcal{X}$  is pure if  $\mathcal{X}_0$  is a zero tensor.

**Definition 7.** (Mode- $n$  unfolding [15]) For an  $N$ th-order quaternion tensor  $\mathcal{X} \in \mathbb{H}^{I_1 \times I_2 \times \dots \times I_N}$ , its mode- $n$  unfolding is denoted by  $\dot{\mathbf{X}}_{(n)}$  and arranges the mode- $n$  fibers to be the columns of the quaternion matrix, i.e.,  $\text{unfold}_{(n)}(\mathcal{X}) = \dot{\mathbf{X}}_{(n)} \in \mathbb{H}^{I_n \times I_1 \dots I_{n-1} I_{n+1} \dots I_N}$ . The  $(i_1, i_2, \dots, i_N)$ th entry of  $\mathcal{X}$  maps to the  $(i_n, x)$ th entry of  $\dot{\mathbf{X}}_{(n)}$ , where  $x = 1 + \sum_{p=1, p \neq n}^N (i_p - 1) X_p$  with

$$X_p = \prod_{d=1, d \neq n}^{p-1} I_d.$$

**Definition 8.** (The  $n$ -mode product [29]) The  $n$ -mode product of a quaternion tensor  $\mathcal{X} \in \mathbb{H}^{I_1 \times I_2 \times \dots \times I_N}$  with a quaternion matrix  $\dot{\mathbf{U}} \in \mathbb{H}^{M \times I_n}$  is denoted by  $\dot{\mathcal{Y}} =$

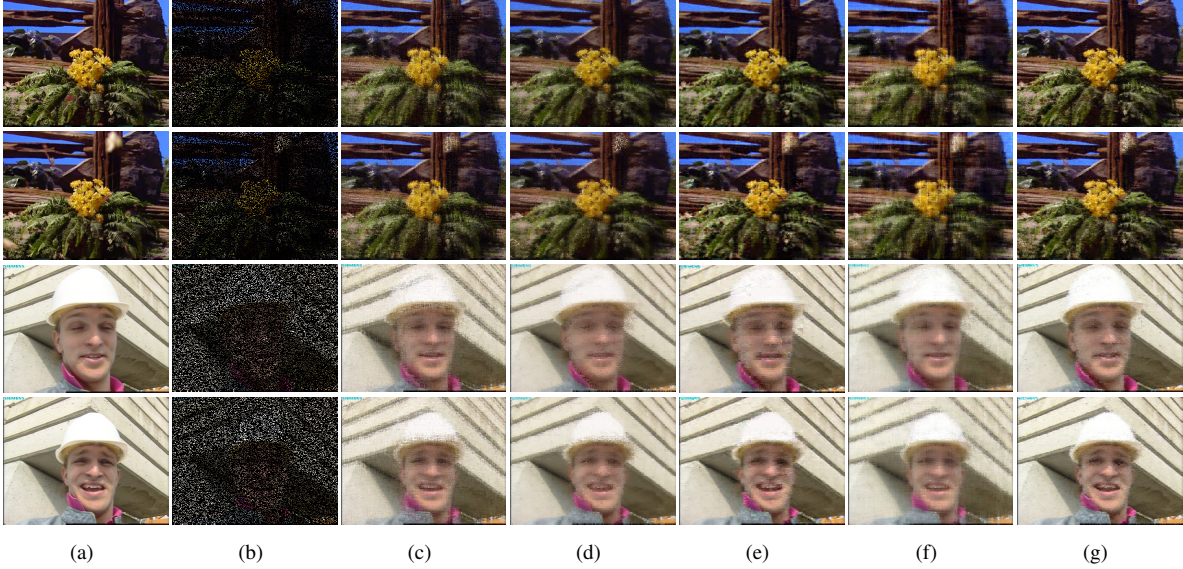


Fig. 9: Recovered two frames of testing color videos for random missing with SR = 20%. From left to right: the original, the observed, and the recovered results by t-SVD, SiLRTC-TT, TMac-TT, LRC-QT, and QTT-SRTD, respectively. From top to bottom: the 1st and 20th frames of “Tempete” and “Foreman”.

$\dot{\mathcal{X}} \times_n \dot{\mathbf{U}} \in \mathbb{H}^{I_1 \times \dots \times I_{n-1} \times M \times I_{n+1} \times \dots \times I_N}$  with entries  $\dot{y}_{i_1 \dots i_{n-1} m i_{n+1} \dots i_N} = \sum_{i_n=1}^{I_n} \dot{u}_{m i_n} \dot{x}_{i_1 i_2 \dots i_N}$ .

One can find more details on quaternions in [15], [23], [28]–[30].

#### APPENDIX B THE PROOF OF THEOREM 1

*Proof.*  $\dot{\mathcal{X}}$  with a QTT decomposition (7) can be represented as

$$\dot{x}_{i_1, i_2, \dots, i_N} = \sum_{l_n=1}^{r_n} \dot{\mathcal{P}}(i_1, \dots, i_n, l_n) \dot{\mathcal{Q}}(l_n, i_{n+1}, \dots, i_N), \quad (35)$$

where  $\dot{\mathcal{P}} \in \mathbb{H}^{I_1 \times \dots \times I_n \times r_n}$  and  $\dot{\mathcal{Q}} \in \mathbb{H}^{r_n \times I_{n+1} \times \dots \times I_N}$ , their entries are calculated by

$$\dot{\mathcal{P}}(i_1, \dots, i_n, l_n) = \sum_{l_1, \dots, l_{n-1}=1}^{r_1, \dots, r_{n-1}} \dot{\mathcal{G}}_1(1, i_1, l_1) \dot{\mathcal{G}}_2(l_1, i_2, l_2) \dots \dot{\mathcal{G}}_n(l_{n-1}, i_n, l_n)$$

$$\dot{\mathcal{Q}}(l_n, i_{n+1}, \dots, i_N) = \sum_{l_{n+1}, \dots, l_{N-1}=1}^{r_{n+1}, \dots, r_{N-1}} \dot{\mathcal{G}}_{n+1}(l_n, i_{n+1}, l_{n+1}) \dots \dot{\mathcal{G}}_N(l_{N-1}, i_N, 1).$$

Equation (35) is equivalent to the following one:

$$\dot{\mathbf{X}}_{[n]} = \dot{\mathbf{P}}_{[n]} \dot{\mathbf{Q}}_{[1]},$$

where  $\dot{\mathbf{P}}_{[n]} \in \mathbb{H}^{\Pi_{j=1}^n I_j \times r_n}$  and  $\dot{\mathbf{Q}}_{[1]} \in \mathbb{H}^{r_n \times \Pi_{j=n+1}^N I_j}$ . Hence, we have

$$\text{rank}(\dot{\mathbf{X}}_{[n]}) = \text{rank}(\dot{\mathbf{P}}_{[n]} \dot{\mathbf{Q}}_{[1]}) \leq r_n.$$

Equality can be achieved following the recursive procedure leading to (8) with minimal  $(r_1, r_2, \dots, r_{N-1})$  in every step described in Remark 1. Specifically, the first step (9) is clearly a rank revealing decomposition of  $\dot{\mathbf{X}}_{[1]}$  so the rank of that quaternion matrix can be used as  $r_1$ . The minimal admissible  $r_2$  in (10) is the rank of  $\dot{\mathbf{H}}_{1[2]}$ . Next, we show that  $\text{rank}(\dot{\mathbf{H}}_{1[2]}) \leq \text{rank}(\dot{\mathbf{X}}_{[2]})$ . Assume  $\dot{\mathbf{z}} \in \mathbb{H}^{\Pi_{j=3}^N I_j \times 1}$  such that  $\dot{\mathbf{X}}_{[2]}\dot{\mathbf{z}} = 0$ . Let  $\dot{\mathbf{y}} = \dot{\mathbf{H}}_{1[2]}\dot{\mathbf{z}}$ , since  $\dot{\mathcal{G}}_1(1, :, :)$  has rank  $r_1$ , then (9) yields  $0 = \sum_{l_1=1}^{r_1} \dot{\mathcal{G}}_1(1, i_1, l_1) \dot{\mathbf{y}}(l_1)$ . Thus,  $\dot{\mathbf{y}} = 0$ , which implies that  $\text{rank}(\dot{\mathbf{H}}_{1[2]}) \leq \text{rank}(\dot{\mathbf{X}}_{[2]})$  indeed holds. Hence,  $r_2 = \text{rank}(\dot{\mathbf{X}}_{[2]})$  by (12). For the subsequent  $r_3, \dots, r_{N-1}$ , one can proceed by using a similar argument.  $\square$

#### APPENDIX C A GENERAL WAY TO GENERATE QUATERNION TRANSFORMS FROM THE CORRESPONDING TRADITIONAL TRANSFORMS

In [31], the authors presented the extension of DCT to the quaternion domain and showed how to calculate the QDCT of a quaternion matrix using its Cayley-Dickson form. In this section, we extend the calculation method of QDCT in [31] to any appropriate quaternion transforms,

*i.e.*, a general way to generate quaternion transforms from the corresponding traditional transforms.

Suppose  $\mathcal{CT}(\cdot)$  is a traditional common transform, then the corresponding quaternion transform  $\mathcal{QT}(\dot{\mathbf{A}})$  for a given quaternion matrix is obtained by the following procedure:

- 1) For a given quaternion matrix  $\dot{\mathbf{A}} \in \mathbb{H}^{M \times N}$ , transform it into the Cayley-Dickson form such that

$$\dot{\mathbf{A}} = \mathbf{C} + \mathbf{D}j,$$

where  $\mathbf{C} \in \mathbb{C}^{M \times N}$  and  $\mathbf{D} \in \mathbb{C}^{M \times N}$  are complex matrices with the same size as  $\dot{\mathbf{A}}$ .

- 2) Calculate  $\mathcal{CT}(\mathbf{C})$  and  $\mathcal{CT}(\mathbf{D})$  respectively, then using them to form a full quaternion matrix, *i.e.*,

$$\dot{\mathbf{A}} = \mathcal{CT}(\mathbf{C}) + \mathcal{CT}(\mathbf{D})j.$$

- 3) Multiply  $\dot{\mathbf{A}}$  with a pure quaternion factor  $\dot{\mu}$  (which satisfies that  $\dot{\mu}^2 = -1$ ) to obtain the final result, *i.e.*,

$$\mathcal{QT}_L(\dot{\mathbf{A}}) := \dot{\mu}\dot{\mathbf{A}} = \dot{\mu}(\mathcal{CT}(\mathbf{C}) + \mathcal{CT}(\mathbf{D})j) \quad (36)$$

or

$$\mathcal{QT}_R(\dot{\mathbf{A}}) := \dot{\mathbf{A}}\dot{\mu} = (\mathcal{CT}(\mathbf{C}) + \mathcal{CT}(\mathbf{D})j)\dot{\mu}. \quad (37)$$

Note that due to the non-commutative multiplication rule of quaternions, the form of  $\mathcal{QT}(\dot{\mathbf{A}})$  has two categories, left-handed form (36) (default form in the paper) and right-handed form (37). Besides, the corresponding inverse transforms can be easily obtained by following similar steps.

## REFERENCES

- [1] Z. Long, Y. Liu, L. Chen, and C. Zhu, "Low rank tensor completion for multiway visual data," *Signal Process.*, vol. 155, pp. 301–316, 2019.
- [2] Z. Zhang and S. Aeron, "Exact tensor completion using t-svd," *IEEE Trans. Signal Process.*, vol. 65, no. 6, pp. 1511–1526, 2017.
- [3] J. A. Bengua, H. N. Phien, H. D. Tuan, and M. N. Do, "Efficient tensor completion for color image and video recovery: Low-rank tensor train," *IEEE Trans. Image Process.*, vol. 26, no. 5, pp. 2466–2479, 2017.
- [4] T. G. Kolda and B. W. Bader, "Tensor decompositions and applications," *SIAM Rev.*, vol. 51, no. 3, pp. 455–500, 2009.
- [5] T. G. Kolda and J. Sun, "Scalable tensor decompositions for multi-aspect data mining," in *Proceedings of the 8th IEEE International Conference on Data Mining (ICDM 2008), December 15-19, 2008, Pisa, Italy*. IEEE Computer Society, 2008, pp. 363–372.
- [6] C. Lu, J. Feng, Y. Chen, W. Liu, Z. Lin, and S. Yan, "Tensor robust principal component analysis with a new tensor nuclear norm," *IEEE Trans. Pattern Anal. Mach. Intell.*, vol. 42, no. 4, pp. 925–938, 2020.
- [7] I. V. Oseledets, "Tensor-train decomposition," *SIAM J. Sci. Comput.*, vol. 33, no. 5, pp. 2295–2317, 2011.
- [8] J. A. Bengua, H. N. Phien, and H. D. Tuan, "Optimal feature extraction and classification of tensors via matrix product state decomposition," in *2015 IEEE International Congress on Big Data, New York City, NY, USA, June 27 - July 2, 2015*, B. Carminati and L. Khan, Eds. IEEE Computer Society, 2015, pp. 669–672.
- [9] Y. Yu, Y. Zhang, and S. Yuan, "Quaternion-based weighted nuclear norm minimization for color image denoising," *Neuro-computing*, vol. 332, pp. 283–297, 2019.
- [10] C. Zou, K. I. Kou, and Y. Wang, "Quaternion collaborative and sparse representation with application to color face recognition," *IEEE Trans. Image Process.*, vol. 25, no. 7, pp. 3287–3302, 2016.
- [11] Y. Chen, X. Xiao, and Y. Zhou, "Low-rank quaternion approximation for color image processing," *IEEE Trans. Image Process.*, vol. 29, pp. 1426–1439, 2020.
- [12] Z. Jia, M. K. Ng, and G. Song, "Robust quaternion matrix completion with applications to image inpainting," *Numer. Linear Algebra Appl.*, vol. 26, no. 4, 2019.
- [13] J. Miao and K. I. Kou, "Color image recovery using low-rank quaternion matrix completion algorithm," *IEEE Trans. Image Process.*, vol. 31, pp. 190–201, 2022.
- [14] L. Yang, J. Miao, and K. I. Kou, "Quaternion-based color image completion via logarithmic approximation," *Inf. Sci.*, vol. 588, pp. 82–105, 2022.
- [15] J. Miao, K. I. Kou, and W. Liu, "Low-rank quaternion tensor completion for recovering color videos and images," *Pattern Recognit.*, vol. 107, p. 107505, 2020.
- [16] J. Wright, Y. Ma, J. Mairal, G. Sapiro, T. S. Huang, and S. Yan, "Sparse representation for computer vision and pattern recognition," *Proc. IEEE*, vol. 98, no. 6, pp. 1031–1044, 2010.
- [17] P. Wang, L. Li, and G. Cheng, "Low-rank tensor completion with sparse regularization in a transformed domain," *Numer. Linear Algebra Appl.*, vol. 28, no. 6, 2021.
- [18] J. Yang, J. Wright, T. S. Huang, and Y. Ma, "Image super-resolution as sparse representation of raw image patches," in *2008 IEEE Computer Society Conference on Computer Vision and Pattern Recognition (CVPR 2008), 24-26 June 2008, Anchorage, Alaska, USA*. IEEE Computer Society, 2008.
- [19] P. Duhamel and M. Vetterli, "Fast fourier transforms: a tutorial review and a state of the art," *Signal processing*, vol. 19, no. 4, pp. 259–299, 1990.
- [20] A. K. Jain, *Fundamentals of digital image processing*. Prentice-Hall, Inc., 1989.
- [21] L. R. Rabiner and B. Gold, "Theory and application of digital signal processing," *Englewood Cliffs: Prentice-Hall*, 1975.
- [22] B. J. Fino and V. R. Algazi, "Unified matrix treatment of the fast walsh-hadamard transform," *IEEE Transactions on Computers*, vol. 25, no. 11, pp. 1142–1146, 1976.
- [23] J. Miao and K. I. Kou, "Quaternion-based bilinear factor matrix norm minimization for color image inpainting," *IEEE Trans. Signal Process.*, vol. 68, pp. 5617–5631, 2020.
- [24] Z. Jia, Q. Jin, M. K. Ng, and X. Zhao, "Non-local robust quaternion matrix completion for large-scale color image and video inpainting," *IEEE Trans. Image Process.*, vol. 31, pp. 3868–3883, 2022.
- [25] J.-H. Yang, X.-L. Zhao, T.-H. Ma, M. Ding, and T.-Z. Huang, "Tensor train rank minimization with hybrid smoothness regularization for visual data recovery," *Applied Mathematical Modelling*, vol. 81, pp. 711–726, 2020.
- [26] J. A. Bengua, H. D. Tuan, H. N. Phien, and M. N. Do, "Concatenated image completion via tensor augmentation and completion," in *10th International Conference on Signal Processing and Communication Systems, ICSPCS 2016, Surfers Paradise, Gold Coast, Australia, December 19-21, 2016*, 2016, pp. 1–7.
- [27] W. Rowan Hamilton, "Ii. on quaternions; or on a new system of imaginaries in algebra," *Phil. Mag., 3rd Ser.*, vol. 25, 01 1844.
- [28] F. ZHANG, "Quaternions and matrices of quaternions," *Linear algebra abd its applications*, vol. 251, pp. 21–57, 1997.

- [29] J. Miao and K. I. Kou, "Quaternion higher-order singular value decomposition and its applications in color image processing," *CoRR*, vol. abs/2101.00364, 2021.
- [30] P. R. Girard, *Quaternions, Clifford Algebras and Relativistic Physics*, 2007.
- [31] W. Feng and B. Hu, "Quaternion discrete cosine transform and its application in color template matching," in *2008 Congress on Image and Signal Processing*, vol. 2. IEEE, 2008, pp. 252–256.